Cell Systems

Article

Enhanced cellular longevity arising from environmental fluctuations

Graphical abstract

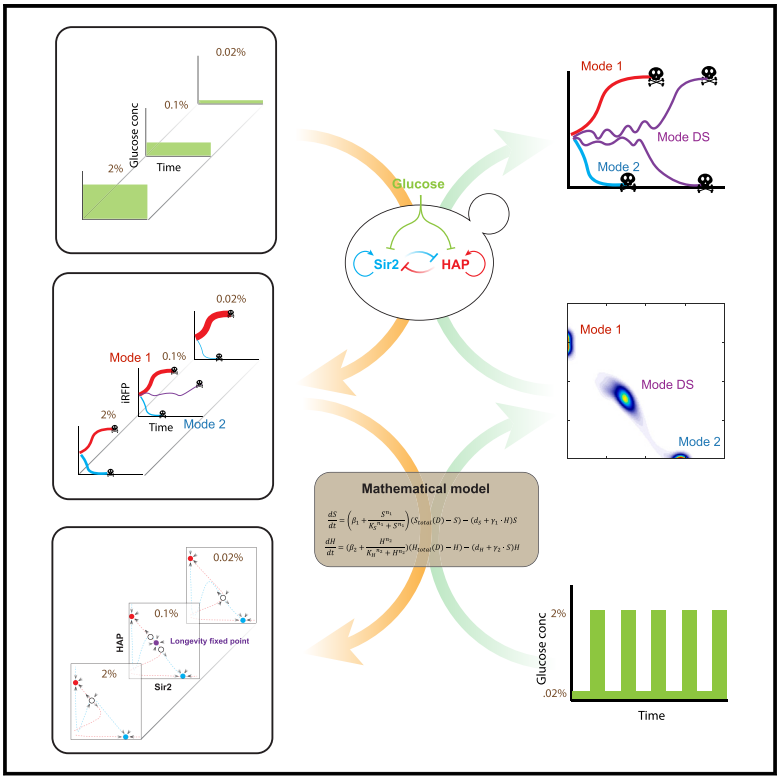

Highlights

- Divergent single-cell aging trajectories are associated with distinct metabolic changes
- External glucose alterations can influence the fate decision of single-cell aging
- External glucose oscillations lead to a new, long-lived mode of aging processes
- Theory suggests stabilizing a "longevity fixed point" as an anti-aging strategy

Authors

Yuting Liu, Zhen Zhou, Hetian Su, ..., Lev S. Tsimring, Jeff Hasty, Nan Hao

Correspondence

zzhou@sioc.ac.cn (Z.Z.), nhao@ucsd.edu (N.H.)

In brief

Cell aging is regulated by interactions of genetic and environmental factors. Combining single-cell imaging experiments and dynamical systems theory, we study glucose modulation of a core gene circuit in yeast aging and propose general principles for longevity—creating a stable, healthy state and dynamically stabilizing it through glucose oscillations.

Liu et al., 2024, Cell Systems *15*, 738–752
August 21, 2024
https://doi.org/10.1016/j.cels.2024.07.007

CellPress

CellPress
OPEN ACCESS

Cell Systems

Article

Enhanced cellular longevity arising from environmental fluctuations

Yuting Liu,[1,4] Zhen Zhou,[1,4,*] Hetian Su,[1] Songlin Wu,[1] Gavin Ni,[1] Alex Zhang,[1] Lev S. Tsimring,[2] Jeff Hasty,[1,2,3] and Nan Hao[1,2,3,5,*]

[1]Department of Molecular Biology, School of Biological Sciences, University of California, San Diego, La Jolla, CA 92093, USA
[2]Synthetic Biology Institute, University of California, San Diego, La Jolla, CA 92093, USA
[3]Department of Bioengineering, University of California, San Diego, La Jolla, CA 92093, USA
[4]These authors contributed equally
[5]Lead contact
*Correspondence: zzhou@sioc.ac.cn (Z.Z.), nhao@ucsd.edu (N.H.)
https://doi.org/10.1016/j.cels.2024.07.007

SUMMARY

Cellular longevity is regulated by both genetic and environmental factors. However, the interactions of these factors in the context of aging remain largely unclear. Here, we formulate a mathematical model for dynamic glucose modulation of a core gene circuit in yeast aging, which not only guided the design of pro-longevity interventions but also revealed the theoretical principles underlying these interventions. We introduce the dynamical systems theory to capture two general means for promoting longevity—the creation of a stable fixed point in the "healthy" state of the cell and the "dynamic stabilization" of the system around this healthy state through environmental oscillations. Guided by the model, we investigate how both of these can be experimentally realized by dynamically modulating environmental glucose levels. The results establish a paradigm for theoretically analyzing the trajectories and perturbations of aging that can be generalized to aging processes in diverse cell types and organisms.

INTRODUCTION

Aging is driven by the accumulation of cellular and genetic damage resulting from intertwined biological processes that are intrinsic to the individual and that are influenced by environmental factors.[1–5] Novel approaches to reduce global healthcare burdens of chronic diseases and aging ultimately demand increased understanding of aging biology and the interactions of the pillars of aging that include diverse yet deeply linked factors such as epigenetics, stress, metabolism, and others.[1,6] Previous studies in model organisms have been focused on measuring lifespan as a static endpoint assay and have identified many genes, the deletion or overexpression of which affects the lifespan.[7–12] An emerging challenge is to understand how these genes interact with one another and operate collectively to drive the aging processes and determine the final lifespan. Because of the intricacies of aging-related processes, traditional reductionist approaches cannot address the totality of such complexity. Instead, new systems-level approaches that integrate stochastic and nonlinear dynamic models with large time-trace datasets are required.

To this end, we set out to quantify and model replicative aging of the budding yeast *Saccharomyces cerevisiae*, a genetically tractable model for aging of mitotic cell types in mammals, such as stem cells. Using microfluidics coupled with time-lapse microscopy,[13,14] we quantitatively tracked the aging processes in a large number of single yeast cells and found that isogenic cells age with two different types of phenotypic changes[15–18]: about half of cells continuously produced daughters, with an elongated morphology during later stages of life (designated as "mode 1" aging). In contrast, the other half produced small, round daughter cells until death (designated as "mode 2" aging). Mode 1 aging is driven by ribosomal DNA (rDNA) silencing loss, resulting in dramatically enlarged and fragmented nucleoli, indicating nucleolar decline.[19] In contrast, mode 2 aging is driven by heme depletion and mitochondrial deterioration.[20]

In yeast, the lysine deacetylase Sir2 mediates chromatin silencing at rDNA to maintain the stability of this fragile genomic locus and the integrity of the nucleolus.[21–24] The heme-activated protein (HAP) complex regulates the expression of genes important for heme biogenesis and mitochondrial function.[25] We previously identified a mutual inhibition circuit of Sir2 and HAP that resembles a toggle switch to mediate the fate decision and divergent progression toward mode 1 vs. mode 2 aging in single cells.[17] Guided by mathematical modeling of the endogenous system, we genetically engineered the Sir2-HAP circuit to reprogram aging trajectories and promote longevity.[17,26] These studies revealed the design principles of genetic circuits for promoting cellular longevity under a static environmental condition. However, how environmental fluctuations impact the dynamical behaviors of genetic circuits to regulate the aging process remains largely unclear.

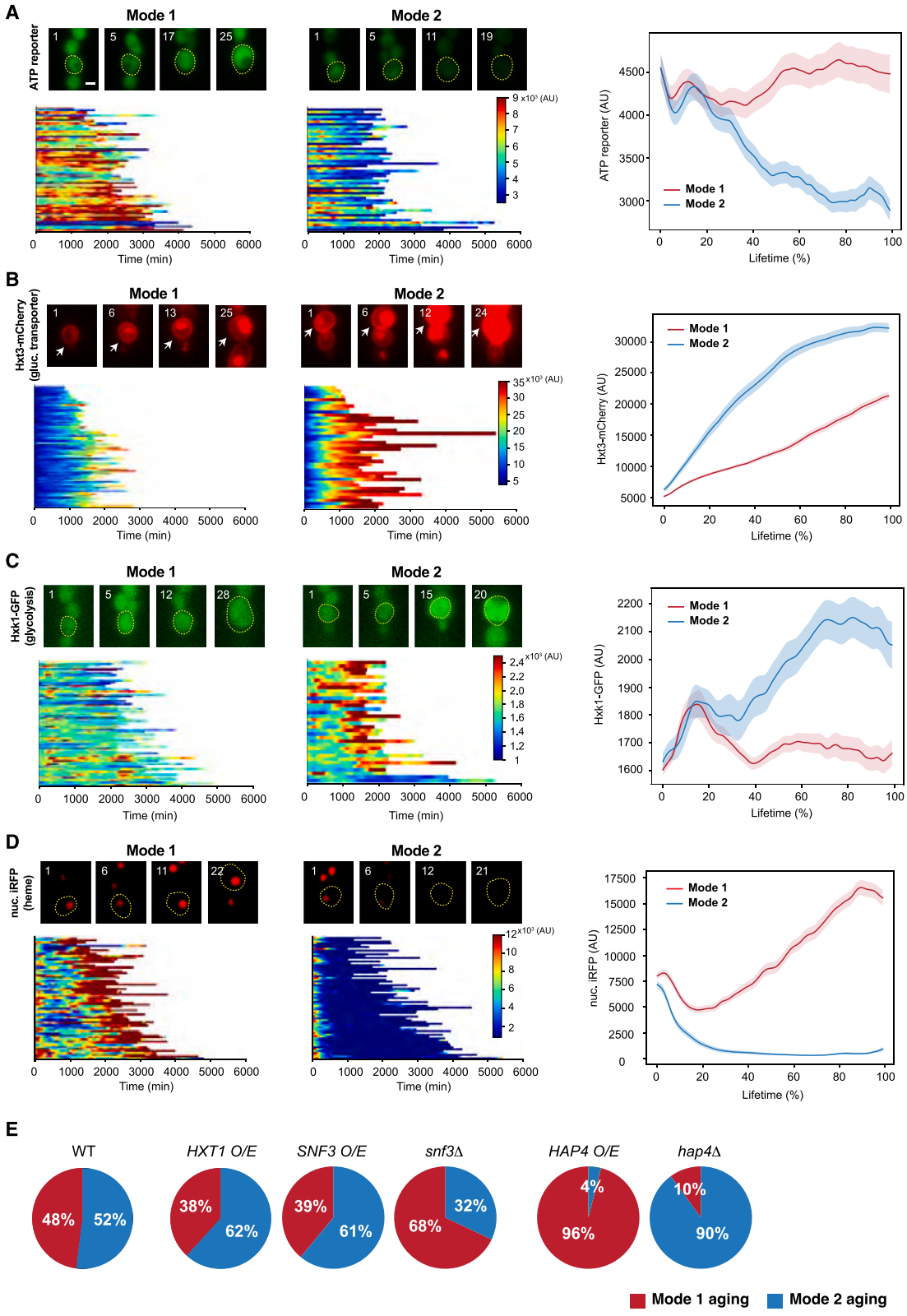

Figure 1. Distinct metabolic changes in mode 1 vs. mode 2 aging

(A–D) Dynamics of an ATP reporter (A, *n* = 116), Hxt3-mCherry (B, *n* = 119), Hxk1-GFP (C, *n* = 115), nuc. iRFP (D, *n* = 120) in mode 1 and mode 2 cells. Top left of each panel: representative time-lapse images of single mode 1 and mode 2 cells. Mother cells are circled in yellow, and the replicative age of the mother cell is

(legend continued on next page)

In this study, we used a mathematical modeling approach to explore the possibility of rationally reprogramming aging by dynamic environmental inputs. A growing number of studies revealed that metabolic alterations are a major hallmark of aging, whereas modulating energy metabolism by environmental factors can dramatically influence the phenotypes and rates of aging.[27–30] For example, caloric restriction (CR) can promote longevity from yeast to mammals.[31–37] Yet, a systematic, quantitative analysis of the impact of environmental factors on the complex networks of aging remain largely missing, making rational reprogramming of aging a challenging task.

Previous studies showed that both Sir2 and HAP are involved in regulating metabolism. For example, Sir2 directly regulates the transcription of multiple metabolic genes at the sub-telomeric regions.[38] The HAP transcriptional complex is responsible for upregulation of respiratory genes and mitochondrial-related genes.[25,39] In addition, the environmental glucose level, which modulates cellular metabolism, can also influence both Sir2 and HAP via different mechanisms. For instance, reduced glucose can enhance the activity of Sir2, a nicotinamide adenine dinucleotide (NAD)-dependent histone deacetylase, by influencing NAD metabolism through multiple routes.[40–44] The expression levels of the HAP components were upregulated upon glucose limiting conditions.[45,46] In agreement with prior results, we found in this study that mode 1 and mode 2 aging, driven by the Sir2-HAP circuit, are associated with distinct metabolic shifts: mode 1 transitions from fermentation to respiration while mode 2 shows increased glycolysis and decreased respiration. We further tracked aging processes in single cells under varying glucose conditions and developed a mathematical model to investigate how environmental glucose alterations influence the dynamical behaviors of the core Sir2-HAP circuit and cellular longevity. Based on single-cell data and dynamical systems theory, we identified two general approaches to extend lifespan by dynamically adjusting environmental glucose inputs—establishing a subtle balance (a stable fixed point) to stabilize the healthy state of the cell and driving dynamic stabilization of the system around this healthy state. Our model not only provides valuable biological insights for designing strategies to promote longevity but also uncovers the underlying theoretical principles behind these strategies, with broad applications across different cell types and organisms.

RESULTS

Metabolic divergence in isogenic aging cells

To determine how aging affects cellular energy production under standard yeast growth conditions, we monitored cellular ATP levels throughout the lifespans of single cells using a genetically encoded fluorescent biosensor containing an ATP-binding pocket linked with a circularly permutated GFP, the fluorescence of which increases with the cellular ATP level.[47] We observed a gradual decline in cellular ATP levels in mode 2, but not mode 1 aging cells (Figure 1A; see STAR Methods and Figure S1 for mode 1 vs. mode 2 classification). To determine the metabolic processes underlying this difference in ATP production among aging cells, we monitored the levels of metabolic factors involved in energy production, such as glycolysis and respiration, and compared their dynamics between mode 1 and mode 2 cells.

We first examined changes in glycolysis during aging by tracking the expression of glucose transporters,[48] a glycolytic enzyme,[49] and the fluorescence of a fructose-1,6-phosphate (FBP) glycolytic flux biosensor.[50] The three glucose transporters we evaluated (Hxt1, Hxt2, and Hxt3) all showed much more dramatically increased expression in mode 2 aging compared with the changes in mode 1 aging (Figures 1B, S2A, and S2B), indicating that a marked elevation in glycolysis occurs specifically during mode 2 aging. Consistent with this observation, the expression of the glycolytic enzyme Hxk1 also increased in mode 2 but not in mode 1 aging (Figure 1C). Moreover, mode 2 aging cells showed a more dramatic increase in the fluorescence of the glycolytic flux biosensor than mode 1 cells (Figure S2C). Heme abundance is an indicator of mitochondrial biogenesis and cellular respiration.[25,51] Using a nuclear-anchored infrared fluorescent protein (nuc. iRFP),[17,52] we tracked heme abundance in single aging cells. The iRFP fluorescence depends on a heme degradation product, biliverdin, and thereby correlates with cellular heme levels.[17] We observed that it gradually elevated in mode 1 aging, but dropped sharply in mode 2 aging (Figure 1D). Together, these results indicated that mode 1 aging features an age-induced transition from fermentation to respiration, in agreement with a previous report,[53] whereas mode 2 aging elicits enhanced glycolysis but suppression of respiration, resulting in a decline in ATP production.

We next asked whether the observed metabolic changes contribute to driving the divergence in mode 1 and mode 2 aging or whether they are simply the consequences of different aging routes. We genetically perturbed the glycolysis or respiration pathway and examined the effects on the fate decision in an isogenic aging population (Figure 1E). We observed that overexpression of the glucose transporter Hxt1 or the glucose sensor Snf3, both of which elevate glucose uptake and glycolysis,[48] promoted mode 2 aging, whereas deletion of Snf3 promoted mode 1 aging. In addition, overexpression of Hap4, which is a major component of the HAP complex (the master transcriptional activator of yeast respiration),[51,54] largely promoted mode 1 aging, whereas deletion of Hap4 promoted mode 2 aging, as previously reported.[17] These results demonstrate that metabolic alterations actively regulate the fate decision of single-cell aging—enhancing respiration or reducing glycolysis promotes mode 1 aging, whereas elevating glycolysis or reducing respiration promotes mode 2 aging.

Taken together, these results demonstrated the interactions between glucose metabolism and the fate decision of aging cells. Based on these findings, we next investigated how

shown at the top left corner of each image. Scale bars, 2 μm. Bottom left of each panel: single-cell color map trajectories in mode 1 and mode 2 cells. Each row represents the time trace of a single cell throughout its lifespan. Color represents the fluorescence intensity as indicated in the color bar. Right of each panel: average fluorescence time traces throughout the life spans in mode 1 and mode 2 cells.

(E) Effects of metabolic gene perturbations on the fate decision in yeast aging. Pie charts show the percentages of mode 1 (red) and mode 2 (blue) in WT and mutants tested. O/E, overexpression.

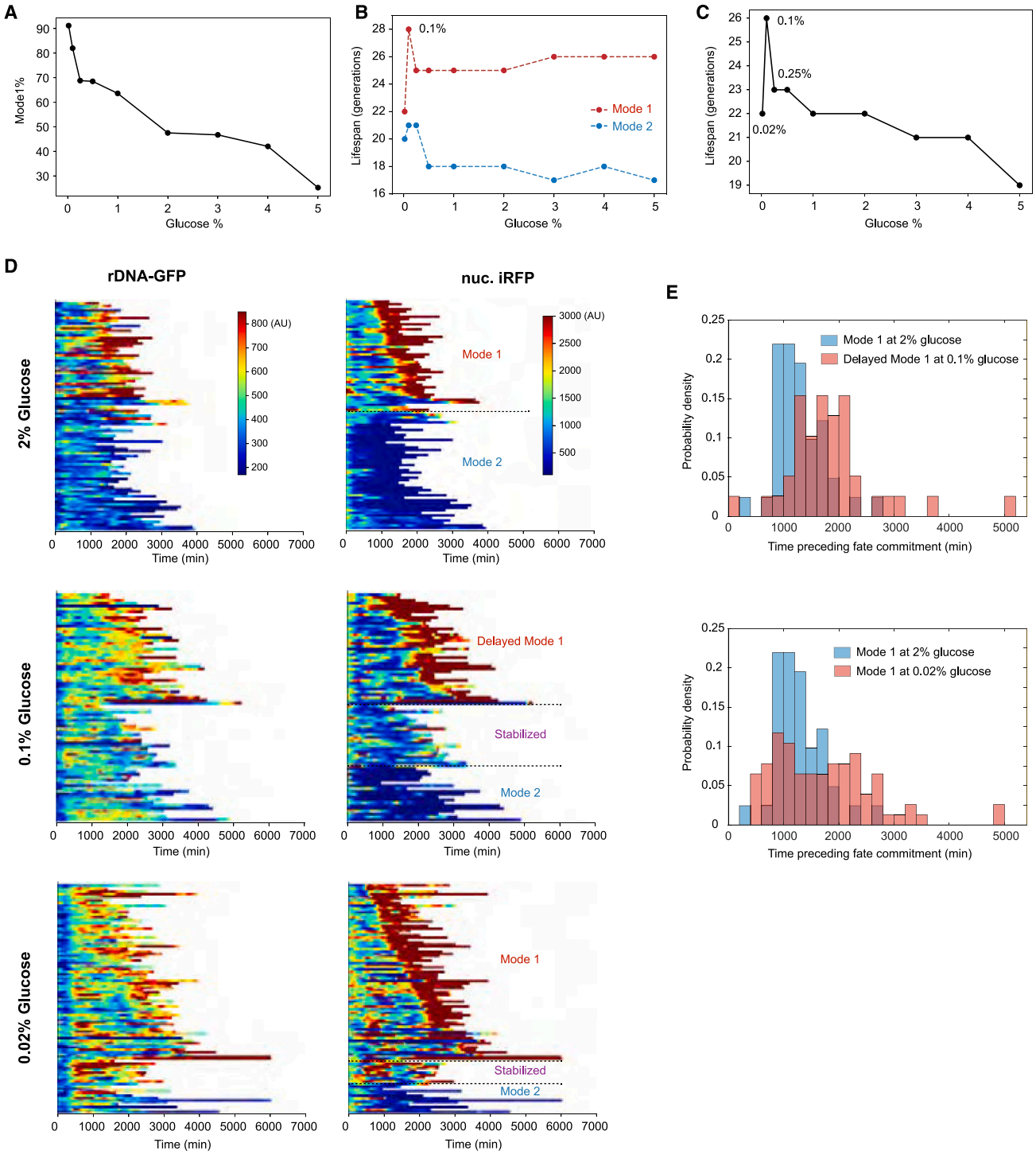

Figure 2. The effects of glucose levels on aging and lifespan

(A) The percentage of mode 1 cells in an aging population as a function of glucose concentration, determined experimentally.

(B) The average lifespans of mode 1 and mode 2 cells as a function of glucose concentration, determined experimentally.

(C) The average lifespan of a whole aging population as a function of the glucose level, determined experimentally. Lifespan curves and statistical analysis are shown in Figure S4.

(D) Single-cell color map trajectories of rDNA-GFP (left) and nuclear-anchored iRFP (right) during aging under different glucose levels, determined experimentally (2% glucose: $n = 91$; 0.1% glucose: $n = 80$; 0.02% glucose: $n = 100$). Each row represents the time trace of a single cell throughout its life span. Color represents the fluorescence intensity as indicated in the color bar. Color maps for rDNA-GFP and nuc. iRFP are from the same cells with the same vertical order. For each glucose level, cells are classified into mode 1 and mode 2 based on their aging phenotypes. Mode 1 cells were further classified into subpopulations based on

(legend continued on next page)

alterations in environmental glucose level, which modulate energy metabolism processes, could influence the fate decision in aging cells and the lifespan.

An optimal level of CR for lifespan extension

Environmental glucose levels can modulate metabolic processes, such as glycolysis and respiration.[55,56] To systematically determine how alterations in glucose levels influence the fate decision in aging and the cellular lifespan, we switched the cell growth medium from the standard 2% glucose condition to different glucose levels at the beginning of aging and tracked the lifespans of single cells (Figure 2; STAR Methods).

We observed that changing glucose levels dramatically affected the fate decision in aging, with decreased glucose promoted mode 1 aging, whereas increased glucose promoted mode 2 aging; the glucose level negatively correlated with the proportions of mode 1 vs. mode 2 in an aging population (Figure 2A). However, the average lifespans within mode 1 and mode 2 aging cells remained relatively unchanged (Figure 2B). The exception was with 0.1% glucose, which markedly extended the lifespans of both mode 1 and mode 2 aging cells. Further decreasing the glucose level to 0.02%, however, largely shortened the lifespan of mode 1 cells (>90% of the population). We confirmed that, in the microfluidic device, the cell cycle rate under 0.02% glucose was comparable to that under the standard 2% glucose condition, suggesting that 0.02% glucose was sufficient to maintain normal cell growth and physiology; thus, the lifespan shortening under 0.02% glucose was not due to the adverse effects of extreme starvation on cell physiology (Figure S3). Hence, 0.1% glucose appeared to be an optimal level of CR that maximally extended the lifespan in yeast (Figure 2C; lifespan curves and t tests are included in Figure S4).

To further define the lifespan-extending effect of the optimal CR conditions, we monitored rDNA silencing loss and heme depletion, two major age-induced deterioration processes that regulate lifespan.[17,26] To track rDNA silencing, we used a GFP reporter inserted within the rDNA (rDNA-GFP).[15] Because expression of the reporter is subject to silencing, increased reporter fluorescence indicates reduced silencing, whereas decreased fluorescence indicates enhanced silencing. To track heme biogenesis, we used a nuclear-anchored iRFP reporter (nuc. iRFP).[52] We observed that, under the standard 2% glucose condition, about half of cells were committed to mode 1 aging that ended life in a state with continuous low rDNA silencing (as indicated by high rDNA-GFP signal) and high-heme biogenesis (as indicated by high iRFP signal), whereas the other half were committed to mode 2 aging and ended life in a state with low heme abundance and high rDNA silencing(Figure 2D, top), consistent with previous reports.[17,26]

In contrast, at 0.1% glucose, the majority (82%) of cells exhibited mode 1 aging. Among these mode 1 cells, 64% showed a substantial time delay preceding fate commitment to the high-heme, low-silencing state (“delayed mode 1” subpopulation in Figures 2D, middle, and S5 for quantifying the time preceding fate commitment using changepoint detection[57,58]), compared with mode 1 cells at 2% glucose (Figure 2E, top). Moreover, the rest (36%) of cells maintained intermediate levels of heme and silencing without a prolonged fate commitment throughout the lifespan and are longer lived (“stabilized” subpopulation in Figure 2D, middle). Decreasing the glucose level to 0.02% further increased the proportion of mode 1 aging cells (91%). However, we observed a wide distribution of fate commitment time, with some cells reaching the high-heme, low-silencing state very early in life (Figures 2D, bottom and 2E, bottom). In addition, the proportion of stabilized subpopulation was largely diminished under this condition. These differences in fate decision dynamics between aging cells under 0.1% and 0.02% glucose are in accord with their lifespan difference (Figure 2C). Together, our results suggest that the maximal lifespan extension under 0.1% glucose could be attributed, at least partially, to the delayed fate commitment to the “aged” states.

The emergence of a longevity fixed point by CR

To quantitatively analyze mechanisms underlying the emergence of an optimal CR condition, we expanded a recently proposed model comprising the mutual inhibition circuit of Sir2 and HAP that resembles a toggle switch to drive the fate decision in yeast aging.[17] Previous studies revealed that CR can elevate the levels of both Sir2 and HAP in yeast.[40–42,45,46] To incorporate these effects in the model, the total amounts of Sir2 and HAP were considered as the functions of the glucose level (Figures 3A and 3B). Thus:

$$\frac{dS}{dt} = \left(\beta_1 + \frac{S^{n_1}}{K_S{}^{n_1}+S^{n_1}}\right)(S_{total}(D) - S) - (d_S + \gamma_1 \cdot H)S \quad \text{(Equation 1)}$$

$$\frac{dH}{dt} = \left(\beta_2 + \frac{H^{n_2}}{K_H{}^{n_2}+H^{n_2}}\right)(H_{total}(D) - H) - (d_H + \gamma_2 \cdot S)H \quad \text{(Equation 2)}$$

Here, S, H are concentrations of active Sir2 and HAP, respectively; β_1, β_2 are basal activation factors of Sir2 and HAP; K_S, K_H are half-activation constants of Sir2 and HAP; d_S, d_H are degradation rates of Sir2 and HAP; γ_1, γ_2 are repression strength of HAP and Sir2; and n_1, n_2 are Hill coefficients for Sir2 and HAP autoregulation. Total amounts of Sir2 and HAP are defined as the functions of glucose concentration D:

$$S_{total}(D) = a_{St}\frac{K_{St}{}^3}{K_{St}{}^3+D^3} + k_{St}D + b_{St} \quad \text{(Equation 3)}$$

$$H_{total}(D) = a_{Ht}\frac{K_{Ht}{}^3}{K_{Ht}{}^3+D^3} + k_{Ht}D + b_{Ht} \quad \text{(Equation 4)}$$

The parameters of the model were estimated by fitting the simulations with the data on the ratios of mode 1 vs. mode 2 under different glucose conditions (Figure S6; Table S1). These

their iRFP dynamics using the changepoints detection method and the time preceding fate commitment was quantified for each mode 1 cell, as illustrated in Figure S5. Different subpopulations were separated by black dashed lines.
(E) Histograms showing the distributions of the time preceding fate commitment among mode 1 cells at different glucose concentrations.

CellPress
OPEN ACCESS

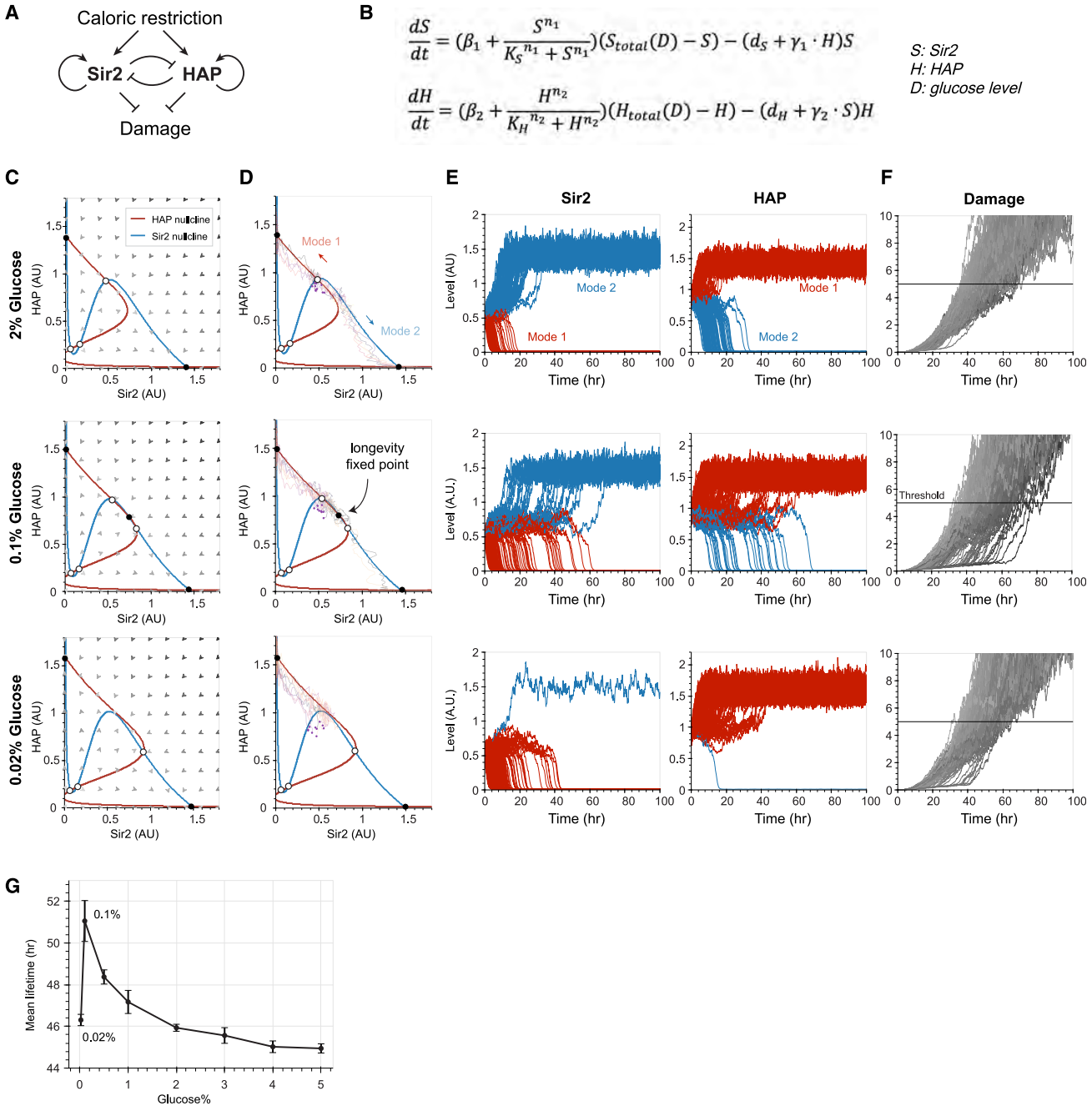

Figure 3. Computational modeling unravels the stability changes of the Sir2-HAP circuit under different glucose levels

(A) Diagram of the circuit topology.

(B) Equations of the model. *S* is the concentration of enzymatically active Sir2, *H* is the concentration of active HAP complex, and *D* is the concentration of glucose. S_{total} and H_{total} are piecewise functions of *D*, representing the total concentration of Sir2 and HAP, respectively (see STAR Methods for details).

(C) Phase planes demonstrate the stability changes of the Sir2-HAP circuit under different glucose levels. The nullclines of Sir2 and HAP are represented in blue and red, respectively. The arrows represent the rate and direction of the system's movement. Fixed points are indicated with open (unstable) and closed (stable) circles. The stable fixed point at the top left corner of each phase plane corresponds to the terminal state of mode 1 aging and the one at the bottom right corner corresponds to the terminal state of mode 2 aging. At 0.1% glucose, a third stable fixed point (longevity fixed point) emerges with intermediate levels of Sir2 and HAP.

(D) Stochastic simulations of aging trajectories on the Sir2-HAP phase planes under different glucose levels. The initial points of each trajectory (purple, $n = 10$) were randomly generated based on the Gaussian distribution for simulation. Trajectories were numerically calculated by the stochastic version of equations from (B).

(E) Stochastic simulations of the Sir2 and HAP time traces during aging under different glucose levels. The initial points ($n = 200$) were randomly generated based on the Gaussian distribution for simulation. Red and blue curves represent the time traces of mode 1 and mode 2 cells, respectively.

(legend continued on next page)

equations were chosen based on the experimental observation that the mode 1 ratio exhibited a switch-like drop from 0.02% to 1% glucose (best described by a Hill function $[\alpha \frac{K^3}{k^3+D^3}]$), followed by a slower gradual decline from 1% to 5% glucose (described by a linear function $[kD + b]$) (Figure S6).

To study the stochastic dynamics of aging, we used the following Langevin equations by adding noise terms to the deterministic equations:

$$\frac{dS}{dt} = \left(\beta_1 + \frac{S^{n_1}}{K_S{}^{n_1}+S^{n_1}}\right)(S_{total}(D) - S) - (d_S + \gamma_1 \cdot H)S + S\xi_S \quad \text{(Equation 5)}$$

$$\frac{dH}{dt} = \left(\beta_2 + \frac{H^{n_2}}{K_H{}^{n_2}+H^{n_2}}\right)(H_{total}(D) - H) - (d_H + \gamma_2 \cdot S)H + H\xi_H \quad \text{(Equation 6)}$$

The noise terms ξ_S, ξ_H are uncorrelated white Gaussian processes with zero mean and autocorrelation $\langle \xi_i(t)\xi_i(t\prime)\rangle = \epsilon_i \delta(t - t'); i \in \{H, S\}$, where $\delta(t - t\prime)$ is Dirac's delta function and ϵ_i is the magnitude of i.

The effects of glucose levels on the dynamics of Sir2 and HAP can be analyzed graphically by plotting the nullclines and vector field in a Sir2-HAP phase plane under different concentrations of glucose (Figures 3C and 3D; Video S1). With the standard 2% glucose level, the system has two stable fixed points—the low Sir2, high HAP point that corresponds to the terminal state of mode 1 aging and the high Sir2, low HAP point that corresponds to the terminal state of mode 2 aging (Figures 3C and 3D, top). Stochastic simulations showed that roughly equal numbers of cells progressed toward either of these two steady states during aging (Figure 3E, top). When the glucose concentration decreases, an unstable fixed point between the two stable fixed points moves toward the high Sir2, low HAP region, biasing the fate decision toward the low Sir2, high HAP state and thereby mode 1 aging (Video S1). This is consistent with our experimental observations that decreasing glucose level increased the proportion of mode 1 cells in an aging population (data in Figure 2A). When the glucose concentration reaches around 0.1%, a third stable fixed point emerges in the intermediate Sir2, intermediate HAP region of the phase plane (Figures 3C and 3D, middle). Stochastic simulations showed that a fraction of cells fluctuated around this new stable fixed point for a period of time before eventually deviating to the low Sir2, high HAP or high Sir2, low HAP states, driven by the noise (Figure 3E, middle). This is consistent with our experimental observations of the delayed mode 1 and stabilized subpopulations of aging cells under the optimal 0.1% glucose condition (simulations in Figure 3E, middle vs. data in Figures 2D middle and 2E, top). This new stable fixed point requires a subtle balance between Sir2 and HAP and hence disappears quickly when the glucose concentration is further decreased (Figures 3C and 3D, bottom). As a result, at 0.02% glucose, the majority of cells aged with mode 1 aging and approached the low Sir2, high HAP state with a wide distribution of commitment time (Figure 3E, bottom). This is consistent with our experimental results of fate commitment dynamics under this condition (simulations in Figure 3E, bottom vs. data in Figures 2D, bottom and 2E, bottom).

To simulate the effects of glucose alterations on lifespan, we linked the Sir2-HAP circuit to cell death using a paradigmatic model framework, recently developed by Uri Alon's group,[59,60] in which the aging process is described as a competition between accelerating damage accumulation and saturating damage removal. The cell death occurs when the level of intracellular damage exceeds a certain threshold value. In our model, we assume that the damage removal rate is dependent on the levels of Sir2 and Hap4. Specifically, the equation for the damage ψ is written as follows:

$$\frac{d\psi}{dt} = \eta t - \frac{S^2}{S^2+K_1{}^2}\frac{H^2}{H^2+K_2{}^2}\psi + \psi\xi_\psi \quad \text{(Equation 7)}$$

Here, η is the production rate of damage and ξ_ψ is the Gaussian white noise term with strength ϵ_ψ. Initial conditions for Sir2 and HAP follow a Gaussian probability distribution $(2\pi\sigma_S\sigma_H)^{-1} exp\left[-\frac{(S-S_0)^2}{\sigma_S^2} - \frac{(H-H_0)^2}{\sigma_H^2}\right]$ (see Table S1 for the parameters of simulations).

Decreasing either Sir2 or HAP levels reduces damage repair/removal and thereby accelerates damage accumulation. The lifetime of a cell is calculated as the time taken for its damage level to hit the threshold (Figure 3F). Because the cell's lifetime and replicative lifespan are positively correlated in general, for the sake of simplicity, our model uses this simulated lifetime as a proxy for lifespan. We also confirmed that the conclusions of our modeling results are not sensitive to the choice of the damage threshold (STAR Methods and Figure S7).

The optimal CR condition allows for the system to spend an extended period near the new stable fixed point with intermediate Sir2 and HAP levels and, hence, to slow damage accumulation, leading to the maximally extended lifespan across different glucose levels (simulations in Figure 3G vs. data in Figure 2C). We therefore designated this stable fixed point as a longevity fixed point. Notably, the emergence of the intermediate stable fixed point (the longevity fixed point in this study) is a well-established, robust feature for the toggle switch network (Equations 1 and 2; mutual inhibition + autoregulation),[17,61–63] whereas the dependence of Sir2 and HAP on glucose level (Equations 3 and 4) is sensitive to parameter choices and is constrained by the data fitting (Figure S6). Further parameter analysis and a discussion of the robustness of the model were included in Figure S8 and in STAR Methods.

Sir2 overexpression can stabilize the longevity fixed point

To determine the dependence of the longevity fixed point on glucose concentration, we performed a bifurcation analysis of

(F) Simulated time traces of damage accumulation based on Sir2 and HAP dynamics in (E). The cell is considered "dead" once its damage level exceeds the arbitrary threshold (horizontal line).
(G) Simulated lifetime as a function of the glucose concentration. Simulations were performed 5 times with 100 cells for each simulation. The black dots and error bars represent the mean value and standard deviation of simulated lifetimes, respectively.

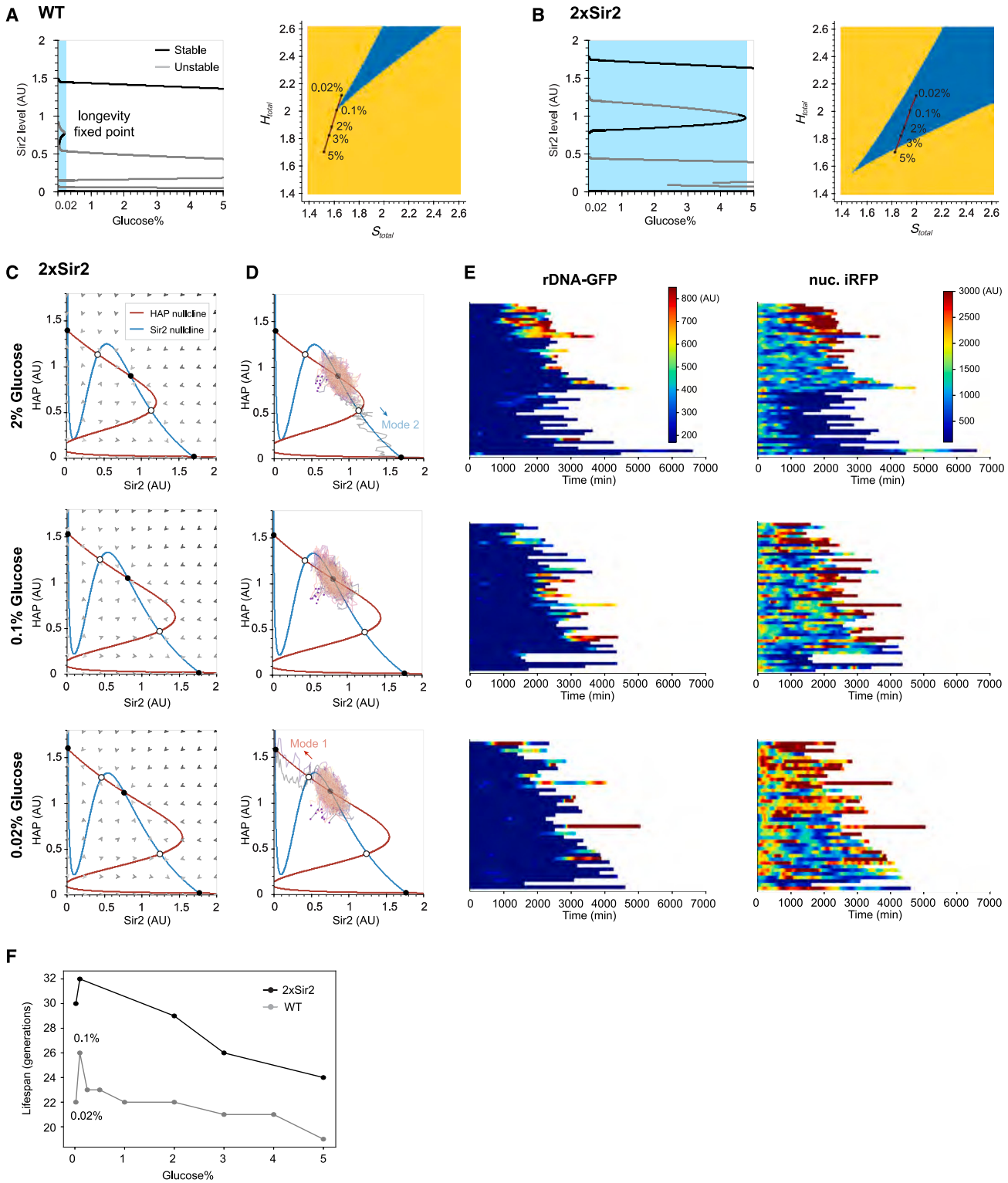

Figure 4. Sir2 overexpression stabilizes the longevity fixed point

(A and B) Modeling analysis of the dependence of the longevity fixed point on the glucose level in WT and 2 × Sir2.

(A and B) Left, Bifurcation analysis for the stability of the Sir2-HAP circuit as a function of the glucose level. Black lines and gray lines represent stable and unstable fixed points, respectively. The range of glucose levels in which the longevity fixed point exists is shaded in blue.

(A and B) Right, the dependence of the longevity fixed point on the total amounts of Sir2 (S_{total}) and HAP (H_{total}). The glucose level can affect the values of S_{total} and H_{total}, which is depicted by the red line. The blue region represents the area where the longevity fixed point exists in the parameter space.

(legend continued on next page)

our model and showed that, in the wild-type (WT) system, the longevity fixed point emerges within a narrow range of glucose levels into which the optimal CR falls (Figure 4A, left). Accordingly, in the Sir2-HAP parameter space, the longevity fixed point exists within a triangular region and the trajectory depicting glucose level changes passes across only the tip of that region (Figure 4A, right).

Our previous analysis of the Sir2-HAP model revealed that 2-fold overexpression of Sir2 can also create the longevity fixed point under standard growth conditions (corresponding to long-lived mode 3 aging).[17] We therefore examined how Sir2 overexpression can alter the dependence of this fixed point on glucose levels. Our model predicted that increasing Sir2 abundance by 2-fold (see STAR Methods) can reshape the phase diagram of the system so that the longevity fixed point can exist within a much wider range of glucose levels and a larger region of the Sir2-HAP parameter space (Figure 4B).

In addition, because the two flanking unstable fixed points are moved further away from the longevity fixed point by Sir2 overexpression, the system becomes less likely to deviate to the other two ''aged'' stable fixed points by the noise (Figures 4C and 4D), which could lead to longer lifespans under a wider range of glucose levels compared with that of WT cells under the optimal CR condition. Changing the glucose level can still modulate the distances between the longevity fixed point and the two flanking unstable fixed points and thereby can influence the probability of deviating to the mode 1 or mode 2 aged state: 2% glucose biased the system toward deviation to the high Sir2, low HAP state and thereby cells have a higher chance to escape from the longevity fixed point and undergo mode 2 aging (Figures 4C and 4D, top), whereas 0.02% glucose biased the system toward the low Sir2, high HAP state and cells have a higher chance to escape to mode 1 aging (Figures 4C and 4D, bottom); 0.1% glucose remained the optimally balanced condition with the least chance of deviations (Figures 4C and 4D, middle).

To test these predictions experimentally, we overexpressed Sir2 by 2-fold and monitored cell aging under different glucose concentrations. In line with a previous study,[17] overexpression of Sir2 dramatically enhances rDNA silencing. Consistent with the model, we also observed substantially delayed rDNA silencing loss and heme elevation during aging of a large fraction of cells under the tested glucose concentrations (0.02%–3%) (Figure 4E), which indicated a more stable rDNA silencing state and thereby longer lifespans than those of WT cells over a wide range of glucose levels (Figure 4F; lifespan curves and t tests are included in Figure S9). These results are in accord with a more stable longevity fixed point in the 2 × Sir2 system. In addition, glucose levels can indeed affect the fate decision (Figure 4E) and lifespan (Figure 4F) in the 2 × Sir2 system, consistent with model simulations (Figure 4D).

External glucose oscillations can enable dynamic stabilization of the aging process

We recently engineered a synthetic Sir2-HAP gene oscillator that could slow cell deterioration, resulting in a dramatically extended lifespan.[26] In this study we considered the possibility that oscillatory glucose inputs may be able to drive dynamic stabilization of the Sir2-HAP circuit and thereby promote longevity. For example, in our model, the system does not have the longevity fixed point at either 2% or 0.02% glucose levels and is unstable in the intermediate Sir2, intermediate HAP range. However, oscillations between 0.02% and 2% glucose levels may be able to restrict the system to that region, reaching a state of dynamic stabilization.

To test this possibility *in silico*, we first performed stochastic simulations with external glucose oscillations between 0.02% and 2%. We found that at least a fraction of cells indeed remain within the intermediate Sir2, intermediate HAP state for an extended period before escaping to the low Sir2 or low HAP states (Figures 5A–5C; Video S2; see STAR Methods and Figure S10 for defining dynamically stabilized [DS] cells from simulations). With increasing input frequency, the proportion of cells that exhibit such a delay increases quickly and then comes to saturation (Figure 5D).

To test these computational predictions experimentally, we integrated our microfluidic device with a computer-controlled electrovalve[64–67] to deliver dynamic patterns of environmental inputs into the culture chambers. We applied external glucose oscillations between 0.02% and 2% over a 6-h period throughout the lifespans of yeast cells and tracked their aging processes. In addition to mode 1 and mode 2 aging cells, we observed that about one-third of cells showed fluctuating rDNA-GFP and iRFP signals for a long period of time before deviating to the low HAP state (Figure 5E). These cells corresponded to the fraction of cells with dynamic stability in our model simulations (Figure 5A, purple curves). We hence designated them as DS cells (see STAR Methods and Figure S11 for the classification of DS cells). These DS cells exhibited waves of rDNA-GFP and iRFP signals driven by glucose inputs and turned out to be very long lived, with an average lifespan of 31 generations, much longer than that of mode 1 or mode 2 cells from the same aging population (Figures 5F and S12, cell cycle lengths for different modes). This DS subpopulation led to a much longer maximal lifespan under glucose oscillations compared with the constant 0.1% glucose condition (55 vs. 45 generations), while the mean lifespan of the whole aging cell population was slightly shorter (24 vs. 26 generations) (Figure S13). We further tested glucose oscillations with an input period of 1, 12, and 24 h. Consistent with the model simulations, increasing input frequency increased the proportion of mode DS cells in an aging population and then the effect reached saturation—reducing the oscillatory period to 1 h modestly affected the proportion of mode DS cells compared with the 6-h period (simulations in

(C) The Sir2-HAP phase planes for 2 × Sir2 under different glucose levels from model simulations.
(D) Stochastic simulations of aging trajectories on the Sir2-HAP phase planes for 2 × Sir2 under different glucose levels.
(E) Experimental data for the dynamics of rDNA-GFP and iRFP during aging. Single-cell color map trajectories of rDNA-GFP (left) and nuc. iRFP (right) for cells with 2-fold overexpression of *SIR2* under different glucose conditions are shown (2% glucose: $n = 53$; 0.1% glucose: $n = 50$; 0.02% glucose: $n = 41$).
(F) The experimentally measured lifespans of WT vs. 2 × Sir2 as a function of the glucose level (0.02% glucose: $n = 45$; 0.1% glucose: $n = 56$; 2% glucose: $n = 59$; 3% glucose: $n = 67$; 5% glucose: $n = 78$).

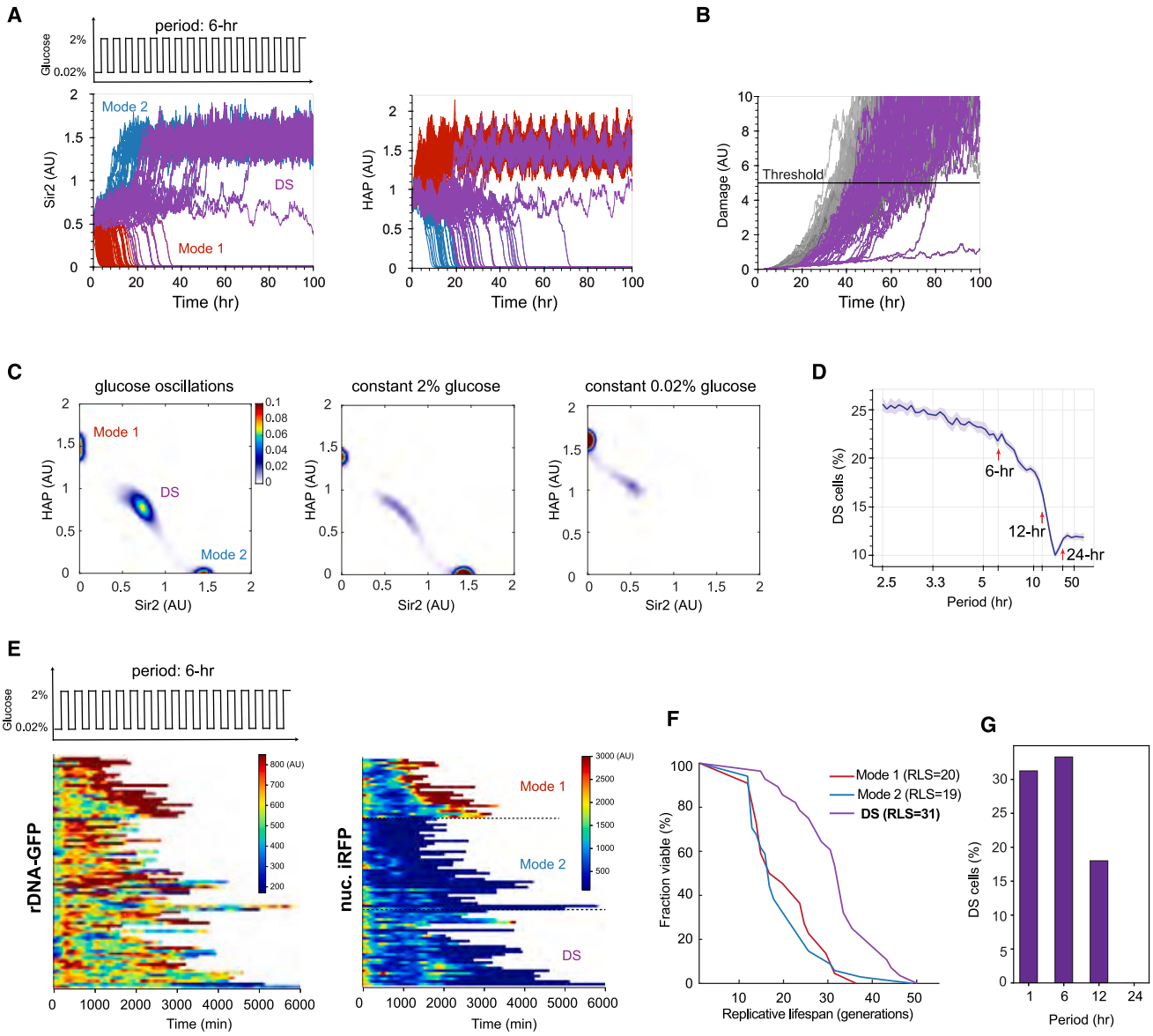

Figure 5. External glucose oscillations enable dynamic stabilization of the aging process

(A) Stochastic simulations of the Sir2 and HAP time traces during aging under glucose oscillations between 0.02% and 2%, with a 6-h period (n = 200). Dynamically stabilized (DS) cells were defined as those that continue to fluctuate around the intermediate Sir2 and HAP state for an extended period before deviation to mode 1 or mode 2 (see STAR Methods). The time traces of DS cells are shown in purple.

(B) Simulated time traces of damage accumulation based on Sir2 and HAP dynamics in (A). The cell is considered dead when its damage level exceeds the arbitrary threshold (horizontal line).

(C) Stability of aging trajectories upon glucose oscillations vs. constant glucose levels. Stochastic simulations were performed in a Sir2-HAP plane of 200 × 200 grids, and the average retention probability in each grid was computed, as indicated by the color bar.

(D) The percentage of DS cells in an aging population as a function of the period of glucose oscillations, from model simulations.

(E) Experimental data for the dynamics of rDNA-GFP and iRFP during aging. Single-cell color map trajectories of rDNA-GFP (left) and nuc. iRFP (right) during aging under glucose oscillations between 0.02% and 2% with a period of 6 h (n = 84) are shown. Each row represents the time trace of a single cell throughout its life span. Color represents the fluorescence intensity as indicated in the color bar. Color maps for rDNA-GFP and nuc. iRFP are from the same cells with the same vertical order. Experiments were repeated independently at least twice. All the cells are classified into mode 1 (top), mode 2 (middle), and DS (bottom), based on TSkmeans algorithm with dynamic time warping (DTW) for clustering (STAR Methods and Figure S11).

(F) Lifespan curves of mode 1, mode 2, and DS cells (n = 84), determined experimentally.

(G) The percentage of DS cells in an aging population as a function of the period of glucose oscillations, determined by experiments (The number of cells analyzed in each group: 1 h, n = 62; 6 h, n = 84; 12 h, n = 84; 24 h, n = 94.).

Figure 5D vs. data in Figures 5G and S14, single-cell aging trajectories upon glucose oscillation with a 1-h period).

Taken together, these results validated our modeling results and demonstrated that external glucose oscillations can indeed enable dynamic stabilization of aging processes, leading to a prolonged lifespan.

DISCUSSION

In this study, using microfluidics and time-lapse microscopy, we tracked the aging trajectories of single yeast cells upon environmental glucose alterations and made several interesting findings: (1) the divergent aging trajectories of single cells are associated with distinct metabolic changes—mode 1 aging features a transition from fermentation to respiration, whereas mode 2 aging features enhanced glycolysis and suppressed respiration. (2) Alterations in environmental glucose concentration can modulate cellular metabolism and thereby influence the fate decision of aging—decreased glucose level leads to a higher ratio of mode 1 vs. mode 2 cells in an aging population, while the lifespan of each mode remains relatively unchanged, with an exception at 0.1% glucose. As glucose alterations were applied after the cells started aging in the microfluidics device, these results indicate that the fate of a young cell is not pre-determined and can be controlled by environmental cues during the early phase of aging, excluding the possibility that mode 2 cells are originated from the pre-existing rho^0 cells that lack mitochondrial DNA in the initial cell population. (3) External glucose oscillations lead to a new long-lived mode of aging process in a fraction of cells.

From the theoretical perspective, we devised a simple mathematical model that can not only reproduce the single-cell aging data under variable glucose conditions but also shed light on the underlying biological mechanisms governing the metabolic regulation of aging. Notably, the model has predictive power that can be used to guide the design of interventional strategies for longevity and to reveal the theoretical principles underlying these strategies. In particular, we focused on the Sir2-HAP toggle switch circuit that mediates the progression of two major aging paths in single yeast cells—one leads to a low Sir2, high HAP state, resulting in nucleolar decline, and the other leads to a high Sir2, low HAP state, causing mitochondrial deterioration (Figure 3).[17] Because both of these terminal states of aging are associated with markedly accelerated damage accumulation, the overall goal for pro-longevity interventions is to avoid, or at least delay, the fate commitment and progression toward these two detrimental steady states (stable fixed points) of the natural aging system. This is challenging in that interventions that elevate either the end of the toggle, Sir2, or HAP will simply push the cell to the other path toward aging and death.

Our model-based analysis here unraveled two general approaches to promote longevity: (1) create and stabilize a longevity fixed point in the healthy intermediate Sir2 and HAP region and (2) enable dynamic stabilization of the system around the healthy state. Both can be realized by modulating environmental glucose levels.

For the first approach, the longevity fixed point, which achieves a subtle balance between Sir2 and HAP at intermediate levels, can be stabilized by either an optimal level of CR or moderate overexpression of Sir2. Both interventions enable the cell to maintain a state with intermediate levels of Sir2 and HAP for an extended period of time. Among them, genetic manipulation of Sir2 leads to a fixed point that is less sensitive to environmental glucose alterations (Figure 4B). Intriguingly, however, although both Sir2 overexpression and CR can delay rDNA silencing loss during aging, their effects on lifespan can still be additive (Figure 4F), suggesting additional mechanisms mediating the effects of CR. In our study, the glucose level, by acting on HAP in addition to Sir2, can modulate the stability of the longevity fixed point generated by Sir2 overexpression and thereby influence the lifespan (Figure 4D). As an immediate application, our model can be used to design the combined treatments with CR and pharmacological activators of sirtuins in which *in silico* simulations could help refine the optimal dosage combinations for maximizing the effects on lifespan extension.

For the second approach, inspired by the nonlinear dynamics and control theory, we adopted the concept of dynamic stabilization for designing pro-longevity strategies. Indeed, an unstable state of a dynamical system, such as the natural aging circuit with intermediate levels of Sir2 and HAP, can be stabilized by applying periodic oscillations of external glucose levels at certain frequencies (Figures 5A and 5B). In a more general sense, *in silico* simulations suggest that swiftly alternating between any pair of inputs whose geometric midpoint resides within the "longevity region" can induce dynamic stabilization. This does not require the presence of a longevity fixed point under static glucose conditions (Figure S15). This implies that, in theory, oscillatory pulses between two glucose levels can stabilize the system in a healthy, long-lived state, whereas the static inputs of either glucose level cannot (Figure 5C). Although our experimental results supported this theory (Figure5E–5G), more comprehensive experimental validations will be needed to further test this idea in a more systematic fashion. It is also interesting to note that this method of dynamical stabilization is reminiscent of the stabilization of an inverted pendulum by periodic vibrations of its pivot point—the so-called Kapitsa's pendulum.[68] Tuning the frequency can modulate the strength of this dynamic stabilization and thereby the proportion of cells that age through this long-lived state of unstable equilibrium (Figure 5D).

Temporally varying metabolic interventions, such as intermittent fasting, are attracting increasing attention as a potential approach to effectively promote longevity and healthspan,[32,34,69,70] but definition of mechanisms underlying their effectiveness remain elusive. Our dynamic stabilization theory of aging, validated here in yeast, may provide the theoretical underpinning for the effects of temporally varying interventions. As large-scale intervention testing is prohibitively time and resource intensive, models based on this theoretical framework can help screen and identify *in silico* the optimal dynamic patterns of metabolic interventions for experimental examinations. Such model-directed approaches can also be applied to identify time-based administration regimes for a series of metabolic intervention compounds named "CR mimetics" (CRMs), including rapamycin, metformin, and spermidine, shown to increase lifespan in multiple model organisms.[71–78]

In addition to the two approaches presented here, a third approach, creating a limit cycle for longevity, was conceived by attempts to modify the circuit structure in the model. Rewiring the mutual inhibition between Sir2 and HAP into a negative

feedback loop can replace the detrimental stable fixed points with a limit cycle on the Sir2-HAP phase plane, leading to sustained oscillations in Sir2 and HAP levels and thereby avoiding fate commitment to either a low Sir2 or low HAP state. This strategy has been realized by genetic circuit engineering in the cell.[26]

We acknowledge that our simple model is only focused on the Sir2-HAP toggle switch and its modulation by glucose. We have omitted many important aging-related pathways, e.g., TORC1 and autophagy pathways, which play crucial roles in mediating the effects of CR on lifespan. As a result, our current model has limitations in reproducing some of the experimental results. For instance, in our model, Sir2 overexpression at 0.1% glucose creates a longevity fixed point that should be very hard to escape from by stochastic simulations (Figure 4D), leading to an extremely long lifespan. However, in experiments, Sir2 overexpression at 0.1% glucose only extended the lifespan to a certain degree (Figures 4E and 4F). Clearly, additional pathways and processes not considered in our model are driving cell aging and death in this mutant. In addition, while our model could predict the emergence of DS cells upon glucose oscillations (Figures 5A–5D), it failed to capture or explain several aspects of the experimental results, including the shortened lifespan of mode 1 cells (Figure 5F, red curve), the initial increase in rDNA-GFP in mode 2 cells (Figure 5E, left), and the slow iRFP waves observed in DS cells (Figure 5E, right). New experimental approaches measuring other related regulatory factors and their interactions with the Sir2-HAP circuit will be needed to obtain mechanistic insights underlying these results and to improve our theoretical understanding of aging. In this study, our goal was to develop a simple theoretical framework that could help us understand several key observations. It will serve as a starting point for more comprehensive experimental and theoretical investigations. When new experimental approaches and data become available, we will refine and expand our model to more accurately simulate and predict the aging processes under varying glucose conditions.

Finally, our model is designed specifically for yeast aging, yet due to its abstract nature, it may be applied to design interventions for any fate decision processes driven by toggle switch circuits, such as trophectoderm differentiation by the Oct3/4-Cdx2 circuit,[79] induced pluripotent stem cell reprogramming by the Oct4-Sox2 circuit,[80] hematopoietic stem cell differentiation by the GATA-1 and PU.1 circuit,[81] and many others. Future studies will be focused on identifying major toggle switch circuits that drive aging in other organisms or in human cells, based on which we can apply our modeling framework to design and test universal interventional strategies for promoting longevity.

STAR★METHODS

Detailed methods are provided in the online version of this paper and include the following:

- KEY RESOURCES TABLE
- RESOURCE AVAILABILITY
  - Lead contact
  - Materials availability
  - Data and code availability
- EXPERIMENTAL MODEL AND STUDY PARTICIPANT DETAILS
- METHOD DETAILS
  - Strain and plasmid construction
  - Setting up microfluidic experiments and time-lapse microscopy
  - Quantification of single-cell aging traces
  - Classification of Mode 1 vs Mode 2 cells
  - Determination of the time preceding fate commitment for Mode 1 aging cells
  - Classification of Mode DS cells
  - Computational Modeling
- QUANTIFICATION AND STATISTICAL ANALYSIS

SUPPLEMENTAL INFORMATION

Supplemental information can be found online at https://doi.org/10.1016/j.cels.2024.07.007.

ACKNOWLEDGMENTS

We thank Dr. Lorraine Pillus for insightful discussions and suggestions on the manuscript. This work was supported by National Institutes of Health R01AG056440 (to N.H., J.H., and L.S.T.), R01GM144595 (to N.H., J.H., and L.S.T.), R01GM111458 (to N.H.), and R01AG068112 (to N.H.).

AUTHOR CONTRIBUTIONS

Conceptualization, Y.L., Z.Z., L.S.T., J.H., and N.H.; methodology, Y.L., Z.Z., L.S.T., J.H., and N.H.; investigation, Y.L., Z.Z., H.S., S.W., G.N., and A.Z.; formal analysis, Y.L., Z.Z., S.W., and L.S.T.; writing—original draft, Y.L., Z.Z., and N.H.; writing—review & editing, Y.L., Z.Z., H.S., S.W., G.N., A.Z., L.S.T., J.H., and N.H.; resources, L.S.T., J.H., and N.H.; supervision, N.H.; funding acquisition, L.S.T., J.H., and N.H.

DECLARATION OF INTERESTS

The authors declare no competing interests.

Received: July 1, 2023
Revised: May 7, 2024
Accepted: July 23, 2024
Published: August 21, 2024

REFERENCES

1. López-Otín, C., Blasco, M.A., Partridge, L., Serrano, M., and Kroemer, G. (2013). The hallmarks of aging. Cell *153*, 1194–1217. https://doi.org/10.1016/j.cell.2013.05.039.
2. Mahmoudi, S., and Brunet, A. (2012). Aging and reprogramming: a two-way street. Curr. Opin. Cell Biol. *24*, 744–756. https://doi.org/10.1016/j.ceb.2012.10.004.
3. McMurray, M.A., and Gottschling, D.E. (2004). Aging and genetic instability in yeast. Curr. Opin. Microbiol. *7*, 673–679. https://doi.org/10.1016/j.mib.2004.10.008.
4. Vijg, J., and Suh, Y. (2013). Genome instability and aging. Annu. Rev. Physiol. *75*, 645–668. https://doi.org/10.1146/annurev-physiol-030212-183715.
5. Melzer, D., Pilling, L.C., and Ferrucci, L. (2020). The genetics of human ageing. Nat. Rev. Genet. *21*, 88–101. https://doi.org/10.1038/s41576-019-0183-6.
6. Kennedy, B.K., Berger, S.L., Brunet, A., Campisi, J., Cuervo, A.M., Epel, E.S., Franceschi, C., Lithgow, G.J., Morimoto, R.I., Pessin, J.E., et al. (2014). Geroscience: linking aging to chronic disease. Cell *159*, 709–713. https://doi.org/10.1016/j.cell.2014.10.039.
7. Kaeberlein, M., and Kennedy, B.K. (2005). Large-scale identification in yeast of conserved ageing genes. Mech. Ageing Dev. *126*, 17–21. https://doi.org/10.1016/j.mad.2004.09.013.
8. Guarente, L., and Kenyon, C. (2000). Genetic pathways that regulate ageing in model organisms. Nature *408*, 255–262. https://doi.org/10.1038/35041700.

9. Kuningas, M., Mooijaart, S.P., van Heemst, D., Zwaan, B.J., Slagboom, P.E., and Westendorp, R.G.J. (2008). Genes encoding longevity: from model organisms to humans. Aging Cell *7*, 270–280. https://doi.org/10.1111/j.1474-9726.2008.00366.x.

10. McCormick, M.A., Delaney, J.R., Tsuchiya, M., Tsuchiyama, S., Shemorry, A., Sim, S., Chou, A.C.Z., Ahmed, U., Carr, D., Murakami, C.J., et al. (2015). A Comprehensive Analysis of Replicative Lifespan in 4,698 Single-Gene Deletion Strains Uncovers Conserved Mechanisms of Aging. Cell Metab. *22*, 895–906. https://doi.org/10.1016/j.cmet.2015.09.008.

11. Fontana, L., Partridge, L., and Longo, V.D. (2010). Extending healthy life span–from yeast to humans. Science *328*, 321–326. https://doi.org/10.1126/science.1172539.

12. Kenyon, C.J. (2010). The genetics of ageing. Nature *464*, 504–512. https://doi.org/10.1038/nature08980.

13. O'Laughlin, R., Jin, M., Li, Y., Pillus, L., Tsimring, L.S., Hasty, J., and Hao, N. (2020). Advances in quantitative biology methods for studying replicative aging in Saccharomyces cerevisiae. Transl. Med. Aging *4*, 151–160. https://doi.org/10.1016/j.tma.2019.09.002.

14. O'Laughlin, R., Forrest, E., Hasty, J., and Hao, N. (2023). Fabrication of Microfluidic Devices for Continuously Monitoring Yeast Aging. Bio Protoc. *13*, e4782. https://doi.org/10.21769/BioProtoc.4782.

15. Li, Y., Jin, M., O'Laughlin, R., Bittihn, P., Tsimring, L.S., Pillus, L., Hasty, J., and Hao, N. (2017). Multigenerational silencing dynamics control cell aging. Proc. Natl. Acad. Sci. USA *114*, 11253–11258. https://doi.org/10.1073/pnas.1703379114.

16. Jin, M., Li, Y., O'Laughlin, R., Bittihn, P., Pillus, L., Tsimring, L.S., Hasty, J., and Hao, N. (2019). Divergent Aging of Isogenic Yeast Cells Revealed through Single-Cell Phenotypic Dynamics. Cell Syst. *8*, 242–253.e3. https://doi.org/10.1016/j.cels.2019.02.002.

17. Li, Y., Jiang, Y., Paxman, J., O'Laughlin, R., Klepin, S., Zhu, Y., Pillus, L., Tsimring, L.S., Hasty, J., and Hao, N. (2020). A programmable fate decision landscape underlies single-cell aging in yeast. Science *369*, 325–329. https://doi.org/10.1126/science.aax9552.

18. Paxman, J., Zhou, Z., O'Laughlin, R., Liu, Y., Li, Y., Tian, W., Su, H., Jiang, Y., Holness, S.E., Stasiowski, E., et al. (2022). Age-dependent aggregation of ribosomal RNA-binding proteins links deterioration in chromatin stability with challenges to proteostasis. eLife *11*. https://doi.org/10.7554/eLife.75978.

19. Sinclair, D.A., Mills, K., and Guarente, L. (1997). Accelerated aging and nucleolar fragmentation in yeast sgs1 mutants. Science *277*, 1313–1316.

20. Hughes, A.L., and Gottschling, D.E. (2012). An early age increase in vacuolar pH limits mitochondrial function and lifespan in yeast. Nature *492*, 261–265. https://doi.org/10.1038/nature11654.

21. Gartenberg, M.R., and Smith, J.S. (2016). The Nuts and Bolts of Transcriptionally Silent Chromatin in Saccharomyces cerevisiae. Genetics *203*, 1563–1599. https://doi.org/10.1534/genetics.112.145243.

22. Kaeberlein, M., McVey, M., and Guarente, L. (1999). The SIR2/3/4 complex and SIR2 alone promote longevity in Saccharomyces cerevisiae by two different mechanisms. Genes Dev. *13*, 2570–2580.

23. Saka, K., Ide, S., Ganley, A.R.D., and Kobayashi, T. (2013). Cellular senescence in yeast is regulated by rDNA noncoding transcription. Curr. Biol. *23*, 1794–1798. https://doi.org/10.1016/j.cub.2013.07.048.

24. Sinclair, D.A., and Guarente, L. (1997). Extrachromosomal rDNA circles–a cause of aging in yeast. Cell *91*, 1033–1042.

25. Buschlen, S., Amillet, J.M., Guiard, B., Fournier, A., Marcireau, C., and Bolotin-Fukuhara, M. (2003). The S. Cerevisiae HAP complex, a key regulator of mitochondrial function, coordinates nuclear and mitochondrial gene expression. Comp. Funct. Genomics *4*, 37–46. https://doi.org/10.1002/cfg.254.

26. Zhou, Z., Liu, Y., Feng, Y., Klepin, S., Tsimring, L.S., Pillus, L., Hasty, J., and Hao, N. (2023). Engineering longevity-design of a synthetic gene oscillator to slow cellular aging. Science *380*, 376–381. https://doi.org/10.1126/science.add7631.

27. Ravera, S., Podestà, M., Sabatini, F., Dagnino, M., Cilloni, D., Fiorini, S., Barla, A., and Frassoni, F. (2019). Discrete Changes in Glucose Metabolism Define Aging. Sci. Rep. *9*, 10347. https://doi.org/10.1038/s41598-019-46749-w.

28. Jazwinski, S.M. (2002). Growing old: metabolic control and yeast aging. Annu. Rev. Microbiol. *56*, 769–792. https://doi.org/10.1146/annurev.micro.56.012302.160830.

29. Azzu, V., and Valencak, T.G. (2017). Energy Metabolism and Ageing in the Mouse: A Mini-Review. Gerontology *63*, 327–336. https://doi.org/10.1159/000454924.

30. Petr, M.A., Alfaras, I., Krawcyzk, M., Bair, W.N., Mitchell, S.J., Morrell, C.H., Studenski, S.A., Price, N.L., Fishbein, K.W., Spencer, R.G., et al. (2021). A cross-sectional study of functional and metabolic changes during aging through the lifespan in male mice. eLife *10*, e62952. https://doi.org/10.7554/eLife.62952.

31. Al-Regaiey, K.A. (2016). The effects of calorie restriction on aging: a brief review. Eur. Rev. Med. Pharmacol. Sci. *20*, 2468–2473.

32. Hwangbo, D.S., Lee, H.Y., Abozaid, L.S., and Min, K.J. (2020). Mechanisms of Lifespan Regulation by Calorie Restriction and Intermittent Fasting in Model Organisms. Nutrients *12*, 1194. https://doi.org/10.3390/nu12041194.

33. Taormina, G., and Mirisola, M.G. (2014). Calorie restriction in mammals and simple model organisms. BioMed Res. Int. *2014*, 308690. https://doi.org/10.1155/2014/308690.

34. Fontana, L., and Partridge, L. (2015). Promoting health and longevity through diet: from model organisms to humans. Cell *161*, 106–118. https://doi.org/10.1016/j.cell.2015.02.020.

35. Liang, Y., Liu, C., Lu, M., Dong, Q., Wang, Z., Wang, Z., Xiong, W., Zhang, N., Zhou, J., Liu, Q., et al. (2018). Calorie restriction is the most reasonable anti-ageing intervention: a meta-analysis of survival curves. Sci. Rep. *8*, 5779. https://doi.org/10.1038/s41598-018-24146-z.

36. Arslan-Ergul, A., Ozdemir, A.T., and Adams, M.M. (2013). Aging, neurogenesis, and caloric restriction in different model organisms. Aging Dis. *4*, 221–232.

37. Li, Y., Daniel, M., and Tollefsbol, T.O. (2011). Epigenetic regulation of caloric restriction in aging. BMC Med. *9*, 98. https://doi.org/10.1186/1741-7015-9-98.

38. Ellahi, A., Thurtle, D.M., and Rine, J. (2015). The Chromatin and Transcriptional Landscape of Native Saccharomyces cerevisiae Telomeres and Subtelomeric Domains. Genetics *200*, 505–521. https://doi.org/10.1534/genetics.115.175711.

39. Mao, Y., and Chen, C. (2019). The Hap Complex in Yeasts: Structure, Assembly Mode, and Gene Regulation. Front. Microbiol. *10*, 1645. https://doi.org/10.3389/fmicb.2019.01645.

40. Anderson, R.M., Bitterman, K.J., Wood, J.G., Medvedik, O., and Sinclair, D.A. (2003). Nicotinamide and PNC1 govern lifespan extension by calorie restriction in Saccharomyces cerevisiae. Nature *423*, 181–185. https://doi.org/10.1038/nature01578.

41. Medvedik, O., Lamming, D.W., Kim, K.D., and Sinclair, D.A. (2007). MSN2 and MSN4 link calorie restriction and TOR to sirtuin-mediated lifespan extension in Saccharomyces cerevisiae. PLoS Biol. *5*, e261. https://doi.org/10.1371/journal.pbio.0050261.

42. Lin, S.J., Kaeberlein, M., Andalis, A.A., Sturtz, L.A., Defossez, P.A., Culotta, V.C., Fink, G.R., and Guarente, L. (2002). Calorie restriction extends Saccharomyces cerevisiae lifespan by increasing respiration. Nature *418*, 344–348. https://doi.org/10.1038/nature00829.

43. Lin, S.J., Ford, E., Haigis, M., Liszt, G., and Guarente, L. (2004). Calorie restriction extends yeast life span by lowering the level of NADH. Genes Dev. *18*, 12–16. https://doi.org/10.1101/gad.1164804.

44. Gallo, C.M., Smith, D.L., Jr., and Smith, J.S. (2004). Nicotinamide clearance by Pnc1 directly regulates Sir2-mediated silencing and longevity. Mol. Cell. Biol. *24*, 1301–1312.

45. DeRisi, J.L., Iyer, V.R., and Brown, P.O. (1997). Exploring the metabolic and genetic control of gene expression on a genomic scale. Science *278*, 680–686.

46. Westholm, J.O., Nordberg, N., Murén, E., Ameur, A., Komorowski, J., and Ronne, H. (2008). Combinatorial control of gene expression by the three yeast repressors Mig1, Mig2 and Mig3. BMC Genomics *9*, 601. https://doi.org/10.1186/1471-2164-9-601.

47. Lobas, M.A., Tao, R., Nagai, J., Kronschläger, M.T., Borden, P.M., Marvin, J.S., Looger, L.L., and Khakh, B.S. (2019). A genetically encoded single-wavelength sensor for imaging cytosolic and cell surface ATP. Nat. Commun. *10*, 711. https://doi.org/10.1038/s41467-019-08441-5.

48. Ozcan, S., and Johnston, M. (1999). Function and regulation of yeast hexose transporters. Microbiol. Mol. Biol. Rev. *63*, 554–569. https://doi.org/10.1128/MMBR.63.3.554-569.1999.

49. Belinchón, M.M., and Gancedo, J.M. (2007). Glucose controls multiple processes in Saccharomyces cerevisiae through diverse combinations of signaling pathways. FEMS Yeast Res. *7*, 808–818. https://doi.org/10.1111/j.1567-1364.2007.00236.x.

50. Monteiro, F., Hubmann, G., Takhaveev, V., Vedelaar, S.R., Norder, J., Hekelaar, J., Saldida, J., Litsios, A., Wijma, H.J., Schmidt, A., and Heinemann, M. (2019). Measuring glycolytic flux in single yeast cells with an orthogonal synthetic biosensor. Mol. Syst. Biol. *15*, e9071. https://doi.org/10.15252/msb.20199071.

51. Zhang, T., Bu, P., Zeng, J., and Vancura, A. (2017). Increased heme synthesis in yeast induces a metabolic switch from fermentation to respiration even under conditions of glucose repression. J. Biol. Chem. *292*, 16942–16954. https://doi.org/10.1074/jbc.M117.790923.

52. Filonov, G.S., Piatkevich, K.D., Ting, L.M., Zhang, J., Kim, K., and Verkhusha, V.V. (2011). Bright and stable near-infrared fluorescent protein for in vivo imaging. Nat. Biotechnol. *29*, 757–761. https://doi.org/10.1038/nbt.1918.

53. Leupold, S., Hubmann, G., Litsios, A., Meinema, A.C., Takhaveev, V., Papagiannakis, A., Niebel, B., Janssens, G., Siegel, D., and Heinemann, M. (2019). Saccharomyces cerevisiae goes through distinct metabolic phases during its replicative lifespan. eLife *8*, e41046. https://doi.org/10.7554/eLife.41046.

54. Forsburg, S.L., and Guarente, L. (1989). Identification and characterization of HAP4: a third component of the CCAAT-bound HAP2/HAP3 heteromer. Genes Dev. *3*, 1166–1178. https://doi.org/10.1101/gad.3.8.1166.

55. Johnston, M. (1999). Feasting, fasting and fermenting. Glucose sensing in yeast and other cells. Trends Genet. *15*, 29–33. https://doi.org/10.1016/s0168-9525(98)01637-0.

56. Rolland, F., Winderickx, J., and Thevelein, J.M. (2002). Glucose-sensing and -signalling mechanisms in yeast. FEMS Yeast Res. *2*, 183–201.

57. Lavielle, M. (2005). Using penalized contrasts for the change-point problem. Signal Process. *85*, 1501–1510. https://doi.org/10.1016/j.sigpro.2005.01.012.

58. Killick, R.F., Fearnhead, P., and Eckley, I.A. (2012). Optimal Detection of Changepoints With a Linear Computational Cost. J. Am. Stat. Assoc. *107*, 1590–1598. https://doi.org/10.1080/01621459.2012.737745.

59. Yang, Y., Karin, O., Mayo, A., Song, X., Chen, P., Santos, A.L., Lindner, A.B., and Alon, U. (2023). Damage dynamics and the role of chance in the timing of E. coli cell death. Nat. Commun. *14*, 2209. https://doi.org/10.1038/s41467-023-37930-x.

60. Karin, O., Agrawal, A., Porat, Z., Krizhanovsky, V., and Alon, U. (2019). Senescent cell turnover slows with age providing an explanation for the Gompertz law. Nat. Commun. *10*, 5495. https://doi.org/10.1038/s41467-019-13192-4.

61. Guantes, R., and Poyatos, J.F. (2008). Multistable decision switches for flexible control of epigenetic differentiation. PLoS Comput. Biol. *4*, e1000235. https://doi.org/10.1371/journal.pcbi.1000235.

62. Huang, S., Guo, Y.P., May, G., and Enver, T. (2007). Bifurcation dynamics in lineage-commitment in bipotent progenitor cells. Dev. Biol. *305*, 695–713. https://doi.org/10.1016/j.ydbio.2007.02.036.

63. Wu, F., Su, R.Q., Lai, Y.C., and Wang, X. (2017). Engineering of a synthetic quadrastable gene network to approach Waddington landscape and cell fate determination. eLife *6*. https://doi.org/10.7554/eLife.23702.

64. Hansen, A.S., Hao, N., and O'Shea, E.K. (2015). High-throughput microfluidics to control and measure signaling dynamics in single yeast cells. Nat. Protoc. *10*, 1181–1197. https://doi.org/10.1038/nprot.2015.079.

65. Hersen, P., McClean, M.N., Mahadevan, L., and Ramanathan, S. (2008). Signal processing by the HOG MAP kinase pathway. Proc. Natl. Acad. Sci. USA *105*, 7165–7170. https://doi.org/10.1073/pnas.0710770105.

66. Jiang, Y., AkhavanAghdam, Z., Li, Y., Zid, B.M., and Hao, N. (2020). A protein kinase A-regulated network encodes short- and long-lived cellular memories. Sci. Signal. *13*, eaay3585. https://doi.org/10.1126/scisignal.aay3585.

67. Hao, N., and O'Shea, E.K. (2011). Signal-dependent dynamics of transcription factor translocation controls gene expression. Nat. Struct. Mol. Biol. *19*, 31–39. https://doi.org/10.1038/nsmb.2192.

68. Blackburn, J.A.S., Smith, H.J.T., and Gro/nbech-Jensen, N. (1992). Stability and Hopf bifurcations in an inverted pendulum. Am. J. Phys. *60*, 903–908. https://doi.org/10.1119/1.17011.

69. Longo, V.D., and Panda, S. (2016). Fasting, Circadian Rhythms, and Time-Restricted Feeding in Healthy Lifespan. Cell Metab. *23*, 1048–1059. https://doi.org/10.1016/j.cmet.2016.06.001.

70. Mattson, M.P., Longo, V.D., and Harvie, M. (2017). Impact of intermittent fasting on health and disease processes. Ageing Res. Rev. *39*, 46–58. https://doi.org/10.1016/j.arr.2016.10.005.

71. Martel, J., Chang, S.H., Wu, C.Y., Peng, H.H., Hwang, T.L., Ko, Y.F., Young, J.D., and Ojcius, D.M. (2021). Recent advances in the field of caloric restriction mimetics and anti-aging molecules. Ageing Res. Rev. *66*, 101240. https://doi.org/10.1016/j.arr.2020.101240.

72. Madeo, F., Carmona-Gutierrez, D., Hofer, S.J., and Kroemer, G. (2019). Caloric Restriction Mimetics against Age-Associated Disease: Targets, Mechanisms, and Therapeutic Potential. Cell Metab. *29*, 592–610. https://doi.org/10.1016/j.cmet.2019.01.018.

73. Selvarani, R., Mohammed, S., and Richardson, A. (2021). Effect of rapamycin on aging and age-related diseases-past and future. GeroScience *43*, 1135–1158. https://doi.org/10.1007/s11357-020-00274-1.

74. Miller, R.A., Harrison, D.E., Astle, C.M., Baur, J.A., Boyd, A.R., de Cabo, R., Fernandez, E., Flurkey, K., Javors, M.A., Nelson, J.F., et al. (2011). Rapamycin, but not resveratrol or simvastatin, extends life span of genetically heterogeneous mice. J. Gerontol. A Biol. Sci. Med. Sci. *66*, 191–201. https://doi.org/10.1093/gerona/glq178.

75. Novelle, M.G., Ali, A., Diéguez, C., Bernier, M., and de Cabo, R. (2016). Metformin: A Hopeful Promise in Aging Research. Cold Spring Harb. Perspect. Med. *6*, a025932. https://doi.org/10.1101/cshperspect.a025932.

76. Mohammed, I., Hollenberg, M.D., Ding, H., and Triggle, C.R. (2021). A Critical Review of the Evidence That Metformin Is a Putative Anti-Aging Drug That Enhances Healthspan and Extends Lifespan. Front. Endocrinol. (Lausanne) *12*, 718942. https://doi.org/10.3389/fendo.2021.718942.

77. Barzilai, N., Crandall, J.P., Kritchevsky, S.B., and Espeland, M.A. (2016). Metformin as a Tool to Target Aging. Cell Metab. *23*, 1060–1065. https://doi.org/10.1016/j.cmet.2016.05.011.

78. Madeo, F., Carmona-Gutierrez, D., Kepp, O., and Kroemer, G. (2018). Spermidine delays aging in humans. Aging (Albany, NY) *10*, 2209–2211. https://doi.org/10.18632/aging.101517.

79. Niwa, H., Toyooka, Y., Shimosato, D., Strumpf, D., Takahashi, K., Yagi, R., and Rossant, J. (2005). Interaction between Oct3/4 and Cdx2 determines trophectoderm differentiation. Cell *123*, 917–929. https://doi.org/10.1016/j.cell.2005.08.040.

80. Shu, J., Wu, C., Wu, Y., Li, Z., Shao, S., Zhao, W., Tang, X., Yang, H., Shen, L., Zuo, X., et al. (2013). Induction of pluripotency in mouse somatic cells

with lineage specifiers. Cell *153*, 963–975. https://doi.org/10.1016/j.cell.2013.05.001.

81. Liew, C.W., Rand, K.D., Simpson, R.J.Y., Yung, W.W., Mansfield, R.E., Crossley, M., Proetorius-Ibba, M., Nerlov, C., Poulsen, F.M., and Mackay, J.P. (2006). Molecular analysis of the interaction between the hematopoietic master transcription factors GATA-1 and PU.1. J. Biol. Chem. *281*, 28296–28306. https://doi.org/10.1074/jbc.M602830200.

82. Keogh, E.J.P., and Pazzani, M.J. (2001). Derivative Dynamic Time Warping. In Proceedings of the 2001 SIAM International Conference on Data Mining, pp. 1–11. https://doi.org/10.1137/1.9781611972719.1.

83. Syakur, M.A.K., Khotimah, B.K., Rochman, E.M.S., and Satoto, B.D. (2018). Integration K-Means Clustering Method and Elbow Method For Identification of The Best Customer Profile Cluster. IOP Conf. Ser.: Mater. Sci. Eng. *336*, 012017. https://doi.org/10.1088/1757-899X/336/1/012017.

STAR★METHODS

KEY RESOURCES TABLE

REAGENT or RESOURCE	SOURCE	IDENTIFIER
Experimental models: Organisms/strains		
BY4741 MATa his3Δ1 leu2Δ0 met15Δ0 ura3Δ0, NHP6a-iRFP-kanMX	Li et al.[15]	NH0268
BY4741 MATa his3Δ1 leu2Δ0 met15Δ0 ura3Δ0, RDN1::NTS1-P_{TDH3}-GFP-URA3,NHP6a-iRFP-kanMX	Li et al.[15]	NH0270
BY4741 MATa his3Δ1 leu2Δ0 met15Δ0 ura3Δ0, RDN1::NTS1-P_{TDH3}-GFP-URA3,NHP6a-iRFP-kanMX, pSIR2::pSIR2-SIR2-HIS3	Li et al.[17]	NH0886
BY4741 MATa his3Δ1 leu2Δ0 met15Δ0 ura3Δ0, NHP6a-iRFP-kanMX, HXT3-mCherry::LEU2; HXT1-CFP::HIS3; HXT2-YFP::URA3	This study	NH1641
BY4741 MATa his3Δ1 leu2Δ0 met15Δ0 ura3Δ0, NHP6a-iRFP-kanMX, pTEF1-iATPSnFR1.0::HIS3	This study	NH1692
BY4741 MATa his3Δ1 leu2Δ0 met15Δ0 ura3Δ0, NHP6a-iRFP-kanMX, pTEFmut7-CggR_R250A-CggRO-YFP::HIS3	This study	NH1704
BY4741 MATa his3Δ1 leu2Δ0 met15Δ0 ura3Δ0, NHP6a-iRFP-kanMX, HXK1-GFP::HIS3	This study	NH1843
Oligonucleotides		
M13@pTEF1: GTAAAACGACGGCCAGTCCA CACACCATAGCTTCAAAAT	This study	Forward primer to PCR TEF1 promoter for making NHB1222
ATPs@pTEF1: ATGAATAGTTTTCATCTTAGA TTAGATTGCTATGCTTTCT	This study	Reverse primer to PCR TEF1 promoter for making NHB1222
pTEF1@ATPs: AATCTAATCTAAGATGAAAAC TATTCATGTTTCTGTTGTT	This study	Forward primer to PCR iATPSnFR1.0 for making NHB1222
M13r@ATP: AAACAGCTATGACTTAATCAAC TTGCAATTTCATT	This study	Reverse primer to PCR iATPSnFR1.0 for making NHB1222
ATP@M13r: TGCAAGTTGATTAAGTCATAGC TGTTTCCTGTGTG	This study	Forward primer to PCR pRS303 plasmid for making NHB1222
pTEF1@M13: ATGGTGTGTGGACTGGCCGT CGTTTTACAAC	This study	Reverse primer to PCR pRS303 plasmid for making NHB1222
303His-I-F: ACGACCATCACACCACTGAA	This study	Forward primer to check integration of pTEF1-iATPSnFR1.0 into genomic HIS3 location
ATP-I-R: CAGCCAATTGCATAGAACCA	This study	Reverse primer to check integration of pTEF1-iATPSnFR1.0 into genomic HIS3 location
BamHI-CggRO-F: CGGGATCCCTGTCGATT CGATACTAACGCCG	This study	Forward primer to PCR CggRO for making NHB1227
EcoRI-CggRO-R: GGAATTCCGAGCTGTACAA GTAGCGTTG	This study	Reverse primer to PCR CggRO for making NHB1227
XhoI-pTEF7-CggR-F: CCGCTCGAGGCGTCGT ACGCTAGGTCGAG	This study	Forward primer to PCR pTEF7-CggR for making NHB1227
EcoRI-pTEF7-CggR-R: GGAATTCTCATTCATC TCTCAACAACTTTTTGGC	This study	Reverse primer to PCR pTEF7-CggR for making NHB1227
HXT1-t-F: TGATGACCAACCATTTTACAAGAGT TTGTTTAGCAGGAAA GGTGACGGTGCTGGTTTA	This study	Forward primer for tagging Hxt1 with fluorescence protein, using pKT series plasmid as template

(*Continued on next page*)

Continued

REAGENT or RESOURCE	SOURCE	IDENTIFIER
HXT1-t-R: ATAAGTCATTAAAATATGCATATTGA GCTTGTTTAGTTTA TCGATGAATTCGAGCTCG	This study	Reverse primer for tagging Hxt1 with fluorescence protein, using pKT series plasmid as template
HXT1-S-F: TCAGCTTCCTGGGTTCCAGTATC	This study	Forward primer to check HXT1-CFP tagging
HXT1-S-R: TGTTGAAGCAGCAGCGTTGT	This study	Reverse primer to check HXT1-CFP tagging
HXT2_tag_F: TGGTAGCTGGATCTCAAAAGAAA AAAGAGTTTCCGAGGAA GGTGACGGTGCTGGTTTA	This study	Forward primer for tagging Hxt2 with fluorescence protein, using pKT series plasmid as template
HXT2_tag_R: AGCCTTAAAAAAATCAGTGCTAGT TTAAGTATAATCTCTTA TCGATGAATTCGAGCTCG	This study	Reverse primer for tagging Hxt2 with fluorescence protein, using pKT series plasmid as template
HXT2_Seq_F: GGTGTCAAACCATGGAAATCTG	This study	Forward primer to check HXT2-YFP tagging
HXT2_Seq_R: ACGTCGAGTCCGTAAGATTTGATC	This study	Reverse primer to check HXT2-YFP tagging
HXT3_tag_F: TGATGACCAGCCATTCTACAAGAAA ATGTTCGGCAAGAAAGGTGACGGTGCTGGTTTA	This study	Forward primer for tagging Hxt3 with fluorescence protein, using pKT series plasmid as template
HXT3_tag_R: AATACACTATTATTCAGCACTACGG TTTAGCGTGAAATTATCGATGAATTCGAGCTCG	This study	Reverse primer for tagging Hxt3 with fluorescence protein, using pKT series plasmid as template
HXT3_seq_F: TGCTAACTACGATGCTGATG	This study	Forward primer to check HXT3-mCherry tagging
HXT3_seq_R: ATTGACTAGCACATCGAATC	This study	Reverse primer to check HXT3-mCherry tagging
HXK1_tag_F: AAGAATTGCCGAAGGTAAGTCTCTTG GTATCATTGGCGCT-GGTGACGGTGCTGGTTTA	This study	Forward primer for tagging Hxk1 with fluorescence protein, using pKT series plasmid as template
HXK1_tag_R: GGGAAAAACACATTTATATTTCATTA CATTTTTTTCATTATCGATGAATTCGAGCTCG	This study	Reverse primer for tagging Hxk1 with fluorescence protein, using pKT series plasmid as template
HXK1_seq_F: ACGATTGTTCCAGCTGAGGA	This study	Forward primer to check HXk1-GFP tagging
HXK1_seq_R: AACATAAGGGCATCACTCAT	This study	Reverse primer to check HXK1-GFP tagging
Recombinant DNA		
pRS303-*pSIR2-SIR2*	Li et al.[17]	NHB0638
pRS303-*pTEF1- iATPSnFR1.0*	This study	NHB1222
pRS303-*TEFmu7-CggR250-CggRO*	This study	NHB1227
Software and algorithms		
Model code in Zenodo	This study	https://doi.org/10.5281/zenodo.11090009
Python 3.11.5	N/A	N/A

RESOURCE AVAILABILITY

Lead contact

Further information and requests for resources and reagents should be directed to and will be fulfilled by the lead contact, Nan Hao (nhao@ucsd.edu).

Materials availability

All the plasmids and yeast strains generated in this study are available upon request.

Data and code availability

- All data reported in this paper will be shared by the lead contact upon request.
- All original code has been deposited at Zenodo.com and is publicly available as the date of publication. DOIs are listed in the key resources table.
- Any additional information required to reanalyze the data reported in this paper is available from the lead contact upon request.

EXPERIMENTAL MODEL AND STUDY PARTICIPANT DETAILS

All yeast strain used in this study were generated from the BY4741 (*MAT*a *his3Δ1 leu2Δ0 met15Δ0 ura3Δ0*) strain background.

METHOD DETAILS

Strain and plasmid construction

Standard protocols were used for molecular cloning. All yeast strain used in this study were generated from the BY4741 (*MAT*a *his3Δ1 leu2Δ0 met15Δ0 ura3Δ0*) strain background. Details of strains, plasmids, and primers are included in key resources table.

To make the *SIR2* 2-fold overexpression plasmid, a XbaI_pSIR2_SIR2_EcoRI fragment containing 620 bp of the *SIR2* promoter + the *SIR2* ORF was made by PCR and then ligated into pRS303, yielding plasmid NHB0638.

To make the plasmid for the ATP reporter, a DNA fragment containing sequences from iATPSnFR$^{1.0}$ (including epsilon subunit, Linkers 1 and 2, GFP sequences)[47] was synthesized by IDT with codon optimization for yeast BY4741. Then PCR and Gibson Assembly were used to insert the 408bp *TEF1* promoter and the iATPSnFR$^{1.0}$ fragment into pRS303 plasmid, yielding NHB1222.

To make the plasmid for glycolysis (FBP) reporter, pHO_pTEFmut7_CggR_R250A_ble (#124585) and pCggRO-reporter (#124582) plasmids were purchased from Addgene.[50] Then forward primer with BamHI cutting site and reverse primer with EcoRI cutting site were used to PCR CggRO sequence. Forward primer with XhoI cutting site and reverse primer with EcoRI cutting site were used to PCR pTEFmut7_CggR_R250A sequences. After that, the two PCR fragments were ligated into pRS303 plasmid cut by XhoI and BamHI to get the plasmid NHB1227.

The yeast strain with the nuc. iRFP reporter (NH268) and the strain with both nuc. iRFP and the NTS1 silencing reporters (NH270) was made as previously described.[15] The yeast strain with the ATP reporter was made by transforming NH268 with DNA fragments from NHB1222 digested by BsmI. The yeast strain with Hxt1-CFP, Hxt2-YFP, Hxt3-mCherry reporters was made by the following steps: firstly, mCherry-LEU2 was amplified by PCR and integrated at the C-terminus of Hxt3 by homologous recombination to make the Hxt3-mCherry strain; secondly, CFP-HIS3 was amplified by PCR and integrated at the C-terminus of Hxt1 by homologous recombination to make the Hxt3-mCherry, Hxt1-CFP strain; Lastly, YFP-URA3 was amplified by PCR and integrated at the C-terminus of Hxt2 by homologous recombination to make the Hxt3-mCherry, Hxt1-CFP, Hxt2-YFP strain. Similarly, the yeast strain with the Hxk1-GFP reporter was made by transforming GFP-HIS3 fragments amplified from PCR. The yeast strain with the glycolysis reporter was made by transforming NH268 with DNA fragments from NHB1227 digested by BsmI.

Setting up microfluidic experiments and time-lapse microscopy

The microfluidic devices and experiments were set up as previously described.[14,15,17,26] The yeast cells were incubated in SC medium containing 2% glucose to an OD600 of 0.8 before loading into the microfluidic devices. SC media containing different concentrations of glucose were delivered to cells via the media supply syringes after cell loading and were applied throughout the experiments. A detailed description of microfluidic fabrication was provided in[14] and a detailed description of setting up a microfluidics aging experiment was provided in.[15]

A computer-controlled electrovalve was used to deliver external glucose oscillations to aging cells in the microfluidic device. The 3-way 0.054 ports electrovalve (The Lee Company, #LFYA1226032H) was connected to a 4-channel USB powered relay module (Numato Lab, SKU: USBPOWRL004). Each channel of the relay could be programmed to control the media input to one microfluidic device by custom-designed MATLAB App. To generate glucose oscillations, growth media with 2% glucose and 0.02% glucose were connected to Port I and O of the electrovalve, respectively, which can be computer-controlled. The outlet port of the valve was connected to the inlet of the microfluidic device.

Time-lapse microscopy experiments were conducted using a Nikon Ti-E inverted fluorescence microscope with an EMCCD camera (Andor iXon X3 DU897). The light source is a spectra X LED system. Images were taken using a CFI plan Apochromat Lambda DM 60X oil immersion objective (NA 1.40 WD 0.13MM). In all experiments, the images were acquired for each fluorescence channel every 15 min for a total of 90 to 120 hours. The exposure and intensity setting for each channel were set as follows: 1) For the glucose tuning assay: Phase 80 ms, GFP 4 ms/30ms at 10% lamp intensity with an EM Gain of 70, and iRFP 50 ms at 15% lamp intensity with an EM Gain of 300; 2) For detecting the ATP reporter: Phase 80 ms, GFP 30ms at 10% lamp intensity with an EM Gain of 70, and iRFP 300ms at 15% lamp intensity with an EM Gain of 300; 3) For detecting Hxt1-3: Phase 80 ms, mCherry 100ms at 25% lamp intensity with an EM Gain of 250, YFP 100ms at 10% lamp intensity with an EM Gain of 250, CFP 60ms at 10% lamp intensity with an EM Gain of 250 and iRFP 300ms at 15% lamp intensity with an EM Gain of 100; 4) For detecting the FBP reporter: Phase 50 ms, YFP 200ms at 10% lamp intensity with an EM Gain of 250, and iRFP 300ms at 15% lamp intensity with an EM Gain of 100.

Quantification of single-cell aging traces

Image processing was conducted using a custom MATLAB code.[15,17,26] The background of images from each fluorescence channel were subtracted. Cell nuclei were masked by thresholding iRFP signal. The mean intensity value of the top 40% of the pixels of fluorescence reporters was quantified, as described previously.[15,17,26] The time traces of reporters were smoothed using the MATLAB function *smoothdata* with specification of the Gaussian method through a 15-element sliding window.

To plot the cell cycle length changes as a function of the percentage of lifetime, the vector of cell cycle length was interpolated to a new vector of 100 elements at evenly distributed 100 query points. Any cells showing obvious abnormal morphologies upon cell

loading were filtered out for replicative lifespan (RLS) analysis. Any cells showing dislocation of reporter mask were filtered out for time trace analysis but included in RLS analysis. Significant numbers for RLS changes were calculated with Gehan-Breslow-Wilcoxon test by using Prism GraphPad 7 (GraphPad Software, CA).

Classification of Mode 1 vs Mode 2 cells

For single-cell data in Figures 1 and 2, Mode 1 and Mode 2 aging cells were classified based on the age-dependent changes in their daughter morphologies, as described in our previous study.[17] Mode 1 cells produce elongated daughters at the late stage of lifespan, whereas Mode 2 cells produce small rounded daughters until death (Figure S1). The classification was further confirmed by iRFP fluorescence (indicating the intracellular heme level). Mode 1 and Mode 2 cells exhibit distinct dynamics of iRFP fluorescence during aging – the iRFP fluorescence increases toward the late stage of Mode 1 aging; in contrast, iRFP signal sharply decreases at the early stage of Mode 2 aging and remains extremely low throughout the entire lifespan (Figure S1). These age-dependent changes in iRFP fluorescence provide robust and quantitative metrics to further confirm the classification of the two aging modes, independent of the need for specific microfluidic devices or imaging setup.

Determination of the time preceding fate commitment for Mode 1 aging cells

For the analysis shown in Figure 2E, Mode 1 cells showed an abrupt and sustained increase of iRFP signal at the late phase of aging, indicating the fate commitment to high HAP, low Sir2 state. To quantitatively determine the time for this fate commitment for each Mode 1 cell, we applied the changepoints detection method described previously (Lavielle et al., 2005; Killick et al., 2012)[57,58] to the iRFP time trace of the cell. The changepoints were calculated with MATLAB *findchangept* function. In function, the option 'statistic' was specified as 'std' and 'MaxNumChanges' was set to 1 for the length of trajectory was less than 2500 min and 1+n for n x 1000 min longer. The last change point was recorded if the 'MaxNumChanges' was larger than 1. A representative iRFP time trace is shown to illustrate the change point identified using this method to be 2001 min in Figure 5S. The change point divides the time trace into two phases: the stable phase (left to the dash line) and the fate commitment phase (right to the dash line). Therefore, this change point is defined as the time preceding fate commitment for a Mode 1 aging cell. Under 0.1% or 0.02% glucose, a subpopulation of Mode 1 cells did not show fate commitment with a sustained increase in the iRFP signal and the change point cannot be detected. Those cells were classified as "stabilized" subpopulation.

Classification of Mode DS cells

For the single-cell time trace data in Figure 5E, the iRFP trajectories were clustered by TSkmeans algorithm with metric of Dynamic Time Warping (DTW)[82] by catching the main dynamic features of the trajectories. Iterating from 2-10 clusters by Elbow method,[83] the optimal number of clusters was determined as 4. Two clusters correspond to Mode 1 and Mode 2 cells, whereas the other two clusters correspond to delayed Mode 1 and delayed Mode 2, which were combined into the DS group (Figure S11). The same analyses were performed to the experimental results from glucose oscillations with different frequencies to classify the DS cells (Figures 5E–5G and S6). The Python packages Tslearn and Yellowbrick were used for clustering and optimal cluster determination, respectively.

Computational Modeling

Stochastic simulations

The stochastic dynamics of aging were studied using the following Langevin equations by adding noise terms to the deterministic equations:

$$\frac{dS}{dt} = \left(\beta_1 + \frac{S^{n_1}}{K_S{}^{n_1} + S^{n_1}}\right)(S_{total}(D) - S) - (d_S + \gamma_1 \cdot H)S + S\xi_S \quad \text{(Equation 5)}$$

$$\frac{dH}{dt} = \left(\beta_2 + \frac{H^{n_2}}{K_H{}^{n_2} + H^{n_2}}\right)(H_{total}(D) - H) - (d_H + \gamma_2 \cdot S)H + H\xi_H \quad \text{(Equation 6)}$$

The noise terms ξ_S, ξ_H are uncorrelated white Gaussian processes with zero mean and autocorrelation $\langle \xi_i(t)\xi_i(t')\rangle = \epsilon_i \delta(t - t'); i \in \{H,S\}$, where $\delta(t - t')$ is Dirac's delta and ϵ_i is the magnitude of i.

To simulate the lifetime of each cell, we coupled the saturated-repair stochastic equation described by [59] with Equations 5 and 6. In Equation 7 below, the rate of damage production rises linearly with time t and damage removal is a saturating function of damage. Considering that the loss of activity in either Sir2 or HAP leads to cell death,[17] we employed the product of Sir2 and HAP saturating functions to represent damage removal. This allows us to simulate the reduction of damage removal capability when the activity of either Sir2 or HAP rapidly decreases. The damage removal term was modified with respect to the level of Sir2 and HAP, the equation is listed as following:

$$\frac{d\psi}{dt} = \eta t - \frac{S^2}{S^2 + K_1{}^2}\frac{H^2}{H^2 + K_2{}^2}\psi + \psi\xi_\psi \quad \text{(Equation 7)}$$

where η is the maximum production rate of damage, ξ_ψ is a Gaussian white noise term with strength ϵ_ψ. The cell was defined as dead when cellular damage ψ reached the threshold which was set to 5 in our cases. Initial conditions for Sir2 and HAP follow a Gaussian probability distribution $(2\pi\sigma_S\sigma_H)^{-1}\, exp\left[-\frac{(S-S_0)^2}{\sigma_S^2}-\frac{(H-H_0)^2}{\sigma_H^2}\right]$ (see Table S1 for the parameters of simulations).

We tested multiple damage thresholds and confirmed that the relative lifetime curves from simulations are not sensitive to the choice of the damage threshold (Figure S7), unless the threshold was set to an extremely high level so that most damage trajectories cannot reach the threshold within the simulation time. We chose the threshold in Figure 3 to best capture the data, but the conclusions of our modeling results do not depend on this choice.

Bifurcation analysis

The fixed points of Equations 1 and 2 were calculated by *fsolve* from SciPy. Points with negative values were omitted. The eigenvalues of Jacobian matrix of Equations 1 and 2 at fixed point were calculated to determine its stability. The sweet spot (the third stable fixed point) was defined as the point that has both negative eigenvalues and lies within the range of 15%-70% of Sir2 and HAP total amount.

Mode ratio determination

Mode 2 was defined as H equals 0 at the end of simulated lifetime. We defined the number of Mode 1 cell equals N-M_2, where the N is the number of overall cells and M_2 is the number of Mode 2 cells. The mode ratio equals $\frac{N-M_2}{N}$.

Parameters fitting

To estimate the parameters for Equations 3 and 4, the randomly generated parameters were recorded until the Manhattan distance (l_1-norm) between simulated mode ratio and experimental mode ratio reached the smallest value for 10 million rounds of simulation (Figure S6). Moreover, to capture the feature of delayed commitment at 0.1% glucose, the mode ratio at 0.1% glucose was calculated only when >10% of the total simulated cells were not committed to either mode until >20hrs, otherwise the mode ratio was defined as infinite. As a result, the probability for not having a longevity fixed point at 0.1% glucose was approximately zero. In other words, it would be nearly 100% chance for the red line to pass the blue region in Figure 4A; for other glucose concentrations, the mode ratio was calculated only when <10% of the cells had delayed commitment after 20 hrs.

The robustness of the model

Regarding the robustness of the model, the emergence of the intermediate stable fixed point (the longevity fixed point in this study) is a well-established, robust feature for the toggle switch network (mutual inhibition + autoregulation).[17,61–63] To illustrate that, we generated 200 groups of parameters for Equations 1 and 2, with random values within a range of 100 folds. For each group of parameters, we generated 1000 sets of H_{total} and S_{total} values randomized between 1 to 20 and evaluated the probability for the emergence of the intermediate stable fixed point. We observed that all the parameter groups can generate the stable fixed point with at least one set of H_{total}-S_{total} values and there are relatively high chances of generating the stable fixed point in the majority of parameter groups (Figure S8). In regard to Figure 4A, the existence of the blue triangle (indicating the emergence of the longevity fixed point) on the H_{total}-S_{total} plane is robust, whereas the red line (indicating the dependence of H_{total} and S_{total} on glucose concentration) is sensitive to parameter choices and is constrained by the data.

Mode DS determination

For model simulations, to get the distributions of lifetime of Mode 1 and Mode 2 cells, 20,000 rounds of simulation were conducted corresponding to the conditions of 0.02% and 2% glucose, respectively. The lifetimes for Mode 1 and Mode 2 were fitted to gamma distributions separately (Figure S10). The threshold in each mode for defining "Mode DS" was set as Cumulative Distribution Function (CDF)=95%.

2 × Sir2 overexpression approximation

When another copy of *SIR2* gene was added, total Sir2 capacity was increased by a factor of κ. Equation 5 became:

$$\frac{dS}{dt} = \left(\beta_1 + \frac{S^{n_1}}{K_S{}^{n_1}+S^{n_1}}\right)(\kappa S_{total}(D) - S) - (d_S + \gamma_1 \cdot H)S + S\xi_S \qquad \text{(Equation 8)}$$

Considering Sir2 is nicotinamide adenine dinucleotide (NAD^+)-dependent enzyme, overexpression of Sir2 may lead to competitive binding of NAD^+, which reduces the inhibition strength (γ_2) to HAP. The assumption is in line with our experimental results in which 2 × Sir2 in 2% glucose condition exhibited no effect on pushing the cells to Mode 2 (~57% mode 1 of 2 × Sir2 vs ~50% mode 1 of WT), indicating a compromise of increase of Sir2 capacity and reduction of Sir2 activity simultaneously. In addition, an extreme overexpression of Sir2 driven by the strong promoter, p*TDH3*, leads to almost 100% mode 1 cells. This suggests that Sir2 does not exert an inhibitory effect on HAP through the loss of Sir2 enzymatic activity, caused by severe competition for NAD^+. To this end, we set κ equals 1.2 and γ_2 equals 0.6.

QUANTIFICATION AND STATISTICAL ANALYSIS

All the information regarding quantification and statistical analysis were included in the figure legends.